Circulation

ORIGINAL RESEARCH ARTICLE

Pathogenesis of Cardiomyopathy Caused by Variants in *ALPK3*, an Essential Pseudokinase in the Cardiomyocyte Nucleus and Sarcomere

Radhika Agarwal, MD, PhD; Hiroko Wakimoto, MD, PhD; Joao A. Paulo, PhD; Qi Zhang, MD; Daniel Reichart, MD; Christopher Toepfer, PhD; Arun Sharma, PhD; Angela C. Tai, BA; Mingyue Lun, MD, PhD; Joshua Gorham, BA; Steven R. DePalma, PhD; Steven P. Gygi, PhD*; J.G. Seidman, PhD*; Christine E. Seidman, MD*

BACKGROUND: *ALPK3* encodes α-kinase 3, a muscle-specific protein of unknown function. *ALPK3* loss-of-function variants cause cardiomyopathy with distinctive clinical manifestations in both children and adults, but the molecular functions of ALPK3 remain poorly understood.

METHODS: We explored the putative kinase activity of ALPK3 and the consequences of damaging variants using isogenic human induced pluripotent stem cell–derived cardiomyocytes, mice, and human patient tissues.

RESULTS: Multiple sequence alignment of all human α-kinase domains and their orthologs revealed 4 conserved residues that were variant only in ALPK3, demonstrating evolutionary divergence of the ALPK3 α-kinase domain sequence. Phosphoproteomic evaluation of both ALPK3 kinase domain inhibition and overexpression failed to detect significant changes in catalytic activity, establishing ALPK3 as a pseudokinase. Investigations into alternative functions revealed that ALPK3 colocalized with myomesin proteins (MYOM1, MYOM2) at both the nuclear envelope and the sarcomere M-band. *ALPK3* loss-of-function variants caused myomesin proteins to mislocalize and also dysregulated several additional M-band proteins involved in sarcomere protein turnover, which ultimately impaired cardiomyocyte structure and function.

CONCLUSIONS: ALPK3 is an essential cardiac pseudokinase that inserts in the nuclear envelope and the sarcomere M-band. Loss of ALPK3 causes mislocalization of myomesins, critical force-buffering proteins in cardiomyocytes, and also dysregulates M-band proteins necessary for sarcomere protein turnover. We conclude that *ALPK3* cardiomyopathy induces ventricular dilatation caused by insufficient myomesin-mediated force buffering and hypertrophy by impairment of sarcomere proteostasis.

Key Words: cardiomyopathy ■ hiPSC-CM ■ M-band ■ phosphoproteomics ■ pseudokinase, α-kinase ■ sarcomere

Cardiomyopathies are prevalent and serious primary diseases of the heart muscle that cause premature morbidity and mortality from progressive heart failure or sudden cardiac death. Approximately half of cardiomyopathies have a genetic etiology with >50 identified disease genes. In adults, many of these genes encode sarcomere and cytoskeletal proteins, whereas in children, cardiomyopathy genes often encode neuromuscular, metabolic, and mitochondrial proteins.[1] Pathogenic variants in cardiomyopathy genes primarily trigger 1 of 2 dichotomous cardiac morphologies: hypertrophy (increased ventricular wall thickness and mass with reduced chamber volumes) or dilatation (normal ventricular wall thickness and increased chamber volumes).[2]

One recently described cardiomyopathy arises from variants in *ALPK3,* which encodes the muscle-specific

Correspondence to: Christine E. Seidman, MD, NRB 256, Deptartment of Genetics, Harvard Medical School, 77 Ave Louis Pasteur, Boston, MA 02115. Email cseidman@genetics.med.havard.edu

*S.P. Gygi, J.G. Seidman, and C.E. Seidman contributed equally.

Supplemental Material is available at https://www.ahajournals.org/doi/suppl/10.1161/CIRCULATIONAHA.122.059688.

For Sources of Funding and Disclosures, see page 1691.

Clinical Perspective

What Is New?

- Damaging variants in *ALPK3* (α-kinase 3), encoding an abundant muscle-specific protein, cause both neonatal and adult-onset cardiomyopathies and lead to both ventricular dilatation and hypertrophy.
- Although ALPK3 contains an α-kinase domain, we show that it lacks catalytic activity and is a pseudokinase.
- ALPK3 localizes to both the nuclear envelope of cardiomyocytes and the M-band of the sarcomere, where it regulates the expression and localization of myomesins (MYOM1 [myomesin-1], MYOM2 [myomesin-2]) and additional M-band proteins important for sarcomere protein turnover.

What Are the Clinical Implications?

- *ALPK3* cardiomyopathy may cause impaired contractility and ventricular dilatation because of mislocalization and dysregulation of myomesin proteins, which are critical for force buffering in cardiomyocytes.
- *ALPK3* cardiomyopathy may cause hypertrophy because of dysregulation of key M-band proteins, which are important for sarcomere protein turnover.
- Therapeutic strategies to restore cardiomyocyte force buffering functions and sarcomere protein turnover may ameliorate disease phenotypes in patients with *ALPK3* cardiomyopathy.

Nonstandard Abbreviations and Acronyms

ALPK3	α-kinase 3
CAPN3	calpain 3
DE	differentially expressed
dIC	dual interlobe cleft variant
eEF2K	eukaryotic elongation factor 2 kinase
eGFP	enhanced green fluorescent protein
hiPSC	human induced pluripotent stem cell
hiPSC-CMs	human induced pluripotent stem cell–derived cardiomyocytes
LV	left ventricular
MuRF1/TRIM63	muscle RING-finger protein 1
MYBPC3	myosin-binding protein c
MYH6	α-myosin heavy chain
MYH7	β-myosin heavy chain
MYOM1	myomesin-1
MYOM2	myomesin-2 (M-protein)
sIC	single interlobe cleft variant
TRPM	transient receptor potential cation channel
TTN	titin
WT	wild type

protein α-kinase 3.[3] Recessive *ALPK3* variants (loss-of-function or deleterious missense) cause cardiomyopathy late in gestation or infancy with biventricular dilatation and depressed contractile function.[3–8] Disease progression is often rapid with hemodynamic decompensation and death in childhood. Rare surviving children demonstrate a most atypical sequence of cardiac remodeling: biventricular dilation that transitions to biventricular hypertrophy, whereas contractile function remains profoundly depressed.[6]

Heterozygous *ALPK3* loss-of-function variants are also estimated to cause ~1.5% to 2.5% of unexplained ventricular hypertrophy that occurs in adults.[6,9] These heterozygous variants likely have variable and age-dependent penetrance, because obligate carrier relatives of critically ill infants with recessive *ALPK3* cardiomyopathy often have no cardiac disease.[6]

ALPK3 encodes a 201-kD protein that contains a nuclear localization signal, 2 immunoglobulin-like domains, and a C-terminal α-kinase domain (Figure 1A). The α-kinase family, a subfamily of the atypical protein kinases, has 6 members in humans: TRPM6 and TRPM7 (transient receptor potential cation channels 6 and 7); eEF2K (eukaryotic elongation factor 2 kinase); and ALPK1, ALPK2, and ALPK3 (α-kinases 1, 2, and 3).[10,12]

ALPK3 was initially discovered during in vitro screens for genes that were expressed in advance of key early cardiac transcription factors (NKX2-5, GATA-4).[13] In situ hybridization studies in developing mice confirmed that *ALPK3* is expressed in the early embryonic cardiac crescent and remains highly expressed in cardiomyocytes throughout life.[13] *Alpk3*-null (*Alpk3*$^{-/-}$) mice, generated by gene trapping, are born at normal Mendelian ratios and are viable and fertile despite biventricular hypertrophy and dilation with reduced contractility.[14]

Despite its primordial and persistent cardiac expression and clear role in cardiomyopathy pathogenesis, the molecular functions and putative kinase activity of ALPK3 remain unknown. To investigate these properties, we introduced *ALPK3* variants in isogenic human induced pluripotent stem cells (hiPSCs) that either produced targeted missense residues in the α-kinase domain or reduced ALPK3 expression. The molecular and functional effects of these variants were first characterized in hiPSC-derived cardiomyocytes (hiPSC-CMs) and then validated in a new *Alpk3* mutant mouse model and in human *ALPK3* patient tissues. Our studies reveal that the kinase domain of ALPK3 lacks catalytic activity but is important for regulating the activities of key force-buffering myomesin proteins in both the nucleus and the sarcomere.

METHODS

The authors declare that all supporting data are available within the article and its Supplemental Material.

Human Induced Pluripotent Stem Cells

PGP1 enhanced green fluorescent protein (eGFP)–titin (TTN) is a male human pluripotent stem cell line with an eGFP tag engineered on the N terminus of TTN, which inserts at sarcomere Z-discs.[15] Tissue culture dishes (6-well) (Fisher Scientific, 07-200-83) were coated with BD Matrigel (BD Biosciences, 354277) at a 1:320 dilution in DMEM F12 (Invitrogen, 11330057). hiPSCs were seeded on Matrigel-coated tissue-culture dishes at ~30% confluency with daily media replacement (mTESR1, STEMCELL Technologies). hiPSCs were passaged every 3 to 4 days, using 0.5 mM EDTA in PBS, so as to not exceed a confluency of 80%. Cell viability after passaging was improved by including 10 μM ROCK inhibitor Y-27632 (R&D Systems, 125410) in culture media for 1 day after passage. Cells were cultured under sterile conditions, and maintained at 37°C, 5% CO_2.[15]

HEK293T

HEK293T cells were grown in DMEM (Invitrogen 11995-073) supplemented with 10% fetal bovine serum (FBS) (ATCC 30-2020) and maintained at 37°C, 5% CO_2.

Mice

Mice were housed in a pathogen-free facility at the New Research Building at Harvard Medical School, fed ad libitum on a 14-hour/10-hour light/dark cycle, and checked daily by veterinary staff. All in vivo experiments were carried out in accordance with the Institutional Animal Care and Use Committee guidelines reviewed and approved under the Institutional Animal Care and Use Committee guidelines at Harvard Medical School. Adult C57BL/6N-Alpk3$^{tm1b(EUCOMM)Hgmu}$/H were obtained from Medical Research Council Harwell, and all mice were at least doubly housed. Genomic DNA was extracted, and genotypes were confirmed using polymerase chain reaction with the KOD Hot Start DNA polymerase kit using 3 primers (forward primer: 5' CTCCTTGAGGGTTAGCTGCCTT 3', reverse primer (wild type [WT]): 5' CCTGTGACAATGCAGGTGAACC 3', reverse primer (*Alpk3*-null) 5' CTACCCCAGACCTTGGGACCA 3'), an annealing temperature of 54°C, and extension time of 40 s for 35 cycles.

Echocardiograms were conducted at birth and periodically throughout life. Mice were euthanized, and a 4-chamber cardiac dissection was performed under a dissecting microscope to obtain left ventricular (LV) tissue for subsequent analysis. The sex of all animals was determined either by visual inspection or by *Sry* polymerase chain reaction for postnatal day 0 pups. The sex ratio of litters was balanced, and both males and females were used for all experiments.

Human Tissues

Discarded LV tissues were obtained from patients with *ALPK3* variants undergoing clinically indicated interventions using human subject research protocols, approved by Massachusetts General Brigham. Patients or parents provided written consent and assent, and the study was approved by an institutional review committee. Tissues were processed for single nuclear RNA sequencing as described.[16] Data from diseased hearts were compared with previously reported normal adult human LV tissues.[16]

Multiple Sequence Alignment of the α-Kinase Domain and Structural Models

Clustal Omega[17] was used for multiple sequence alignment of α-kinase domains from all human α-kinases, and their orthologs in multiple species (see UniProt accession IDs in Figure S1). Visualization and analysis of multiple sequence alignment was performed in JalView.[18]

The solved TRPM7 α-kinase domain crystal structure (Protein Data Bank 1IA9_A, refined with Modeller)[11,19] was used to annotate homologous ALPK3 kinase domain residues[10] with University of California San Francisco Chimera.[20]

CRISPR/Cas9 Genome Editing

All guide RNAs and homology-directed repair arms were designed with Benchling. For the *ALPK3* exon 6 guide RNA, used to produce the *ALPK3*$^{ns/del}$ line, a fragment bearing all components necessary for guide RNA expression (U6 promoter + target sequence [AGAAGAATGTGCAGGCAGAT] + guide RNA scaffold + termination signal) was synthesized as a gBlock from Integrated DNA Technologies and cloned into the TOPO plasmid using the Zero Blunt Topo II PCR cloning kit (Invitrogen K2800-02). A combination of 4 μg guide RNA TOPO plasmid and 2 μg Cas9 plasmid (pSpCas9(BB)-2A-Puro [PX459] V2.0; Addgene 62988) was used for genome editing as described previously.[21] *ALPK3* CRISPR RNAs were synthesized as custom ALT-R CRISPR RNA (crRNA) from Integrated DNA Technologies. The crRNA (*ALPK3*$^{dIC/dIC}$ [dIC, dual interlobe cleft variant] targeting sequence: CTCTCTTTTCAGGGGTTGAC; *ALPK3*$^{sIC/sIC}$ [sIC, single interlobe cleft variant] targeting sequence: CAGCTTCCTTGTCACAGACT; *ALPK3*$^{del/del}$ targeting sequence: TACCTGCCAAGTCTGTGACA) was annealed with the 5' ATTO 550 trcRNA to create the guide RNA, which was incubated together with the ALT-R S.p HiFi Cas9 3NLS to create the function ribonucleoprotein complex per Integrated DNA Technologies protocol. The *ALPK3* single strand homology-directed repair templates were synthesized by Integrated DNA Technologies as an Ultramer single strand DNA oligo (*ALPK3*$^{dIC/dIC}$ sequence: AGTATATCTTCCTGCTGGAGA TGTGGGGGCTTAGAGCCAGCCCAGACTGGCATCAACTC CCAACTTTCTCTCTTTTCAGAAGTTGACTGGAAGATGACT GCTGTGCAGATTGCTACCAAACTCCGAGGGTGAGTGG TTCTT; *ALPK3*$^{sIC/sIC}$ sequence: GAGGCTCCGACAGCATCTGG CAGCTCTGAGGCCATGCAGAAATGCCAGACCTTCCAACAC TGGCTGTATCAGTGGACAAATGGCAGCTTCCTTGTCACAG CCCTTGCAGGTACGAGGGTGTGAGGGTGCACGGGTAC GCATGTGCATGGATGTGAAAGCATGCAGAGGAGGCAAAG CCATAGTGCTTGGCTGATCGTTTA; *ALPK3*$^{del/del}$ mutant sequence: GAGGCTCCGACAGCATCTGGCA GCTCTGAGGC CATGCAGAAATGCCAGACCTTCCAACACTGGCTGTATC AGTGGACAAATGGCAGCTTTCTTGTCACAGCCTTGGCAG GTACGAGGGTGTGAGGGTGCACGGGTACGCATGT GCATGGATGTGAAAGCATGCAGAGGAGGCAAAGCCATAG TGCTTGGCTGATCGTTTA).

For nucleofection of CRISPR components, adherent hiPSCs were dissociated with accutase and washed 1× with PBS. Approximately 1×10^6 hiPSCs were resuspended in 82 µL human stem cell nucleofector solution and 18 µL supplement 1 (Lonza). CRISPR components (either guide RNA plasmid + Cas9 plasmid or CRISPR ribonucleoprotein complex + 1 µL 100 µM single strand homology-directed repair template) were added, and the mixture was transferred into an electroporation cuvette and nucleofected using program B-016 on the Amaxa 2B nucleofector (Lonza). For plasmid-based CRISPR, puromycin (Invitrogen A11138-03) selection at a concentration of 0.5 µg/mL was continued for 2 days after nucleofection.[22]

After ~1 week, single rounded colonies were picked under a dissection microscope using sterile pipette tips into a new Matrigel-coated 96-well plate in the presence of 5 µM ROCK inhibitor Y-27632 (R&D Systems 125410).

Genomic DNA was extracted using PrepGEM (VWR PUN0500), and colonies were screened for the presence of gene editing by polymerase chain reaction amplification followed by Sanger sequencing. Colonies with evidence of gene editing were subcloned (≥5 independent clones) to verify clonality. Clonality of populations containing indels were further confirmed by next-generation sequencing analysis (MiSeq, Figure S2).

Ploidy Analysis Using Low-Read Depth Next-Generation Sequencing

Genomic DNA collected from hiPSCs cultured in 1 well of a 6-well plate was extracted with the DNeasy Blood&Tissue kit (Qiagen 69504) per the manufacturer's protocol. DNA quality and concentration were assessed by the Agilent 4200 TapeStation system (Agilent Technologies G2991BA), and 1 ng genomic DNA for each sample was tagmented with the Nextera XT DNA Library prep kit (Illumina, FC-131-1096). Libraries were amplified and cleaned with AMPure XP beads (Agencourt A63882). Equal amounts of libraries were pooled and sequenced, targeting on at least 200,000 reads per sample and mapped to the hg38 reference genome. Bam files were loaded into R studio (version 4.0.1). Raw reads were counted with a fixed bin size of 500 using '*getBinAnnotations()*' and '*binReadCounts ()*' functions, and then normalized to total read counts of corresponding chromosomes. For each chromosome, normalized counts from different samples were visualized in a single plot with the '*plot()*' function for ploidy comparisons (Supplemental Data S5 and S6).

Differentiation of hiPSC-CMs

hiPSCs were differentiated into cardiomyocytes in monolayers as described previously with minimal modification.[23] hiPSCs seeded in Matrigel-coated 6-well culture plates were grown to 90% confluency before initiating the hiPSC-CM differentiation. To initiate differentiation, 18 µM CHIR-99021 (Tocris 44-231-0) in RPMI media (Invitrogen) supplemented with B27 minus insulin (Thermo Fisher Scientific) was added to hiPSCs for 1 day (days 0 to 1). The media was changed to RPMI with B27 minus insulin for 2 days (days 1 to 2). Cultures were then treated with 2 µM Wnt-C59 (Biorbyt orb181132) in RPMI supplemented with B27 minus insulin for 2 days (days 3 to 5). Cells were maintained in RPMI with B27 minus insulin for 2 additional days (days 6 to 7). On day 7, media was changed to RPMI with B27 plus insulin (Invitrogen), and the media were replenished every other day until day 11, at which point cells underwent a 7-day glucose deprivation protocol to enrich for cardiomyocytes; for enrichment, cells were cultured in RPMI media devoid of glucose (Life Technologies) supplemented with B27 with insulin, which was replaced every other day until day 17. On day 17, cells were again cultured in growth media containing glucose (RPMI supplemented with B27 plus insulin) with media replacement every other day. All proteomics and RNA sequencing experiments were performed with hiPSC-CMs at days 30 to 32 of differentiation. All other assays (sarcomere contractility, immunofluorescence) were performed with hiPSC-CMs that were between day 30 and day 40 of cardiomyocyte differentiation.

Evaluation of Sarcomere Contractile Function in hiPSC-CMs

hiPSC-CMs were lifted and replated onto Matrigel-coated glass-bottom imaging-optimized 12-well plates (Mat-Tek) at day 20 of cardiomyocyte differentiation as previously described.[15] hiPSC-CMs were cultured in RPMI B27 plus insulin containing 5 µM ROCK inhibitor and 20% FBS for 2 days after replating, after which they were cultured in RPMI B27 plus insulin until days 30 to 32 when imaging was performed. For video microscopy, hiPSC-CMs were maintained in a heated and humidified chamber (37°C, 5% CO_2) attached to the stage of a fluorescence microscope (Keyence BZ X-710). Five-second videos of sarcomeres in beating hiPSC-CMs (typically clusters of 2 to 4 cells each) were acquired using a 100× oil objective at an acquisition rate of 30 frames per second. Analysis of sarcomere contraction was performed using SarcTrack software.[24]

Transient Transfection of HEK293T Cells

HEK293T cells were grown in 100-mm culture dishes to 80% confluency and transfected with 7.5 µg total plasmid DNA encoding human ALPK3-FLAG (Origene RC220076) using Lipofectamine 3000 (Invitrogen L3000001) per the manufacturer's protocol alongside nontransfected control dishes. Cells were harvested at 72 hours after transfection for analysis.

Harvest of Cell and Tissue Lysate for Western Blotting and Mass Spectrometry

Cells (HEK293T cells/hiPSC-CMs at day 30 of cardiomyocyte differentiation) were washed quickly in cold PBS. Adherent cells were scraped from the tissue culture dish (100-mm plate for HEK293T cells, all wells of a 6-well culture dish for hiPSC-CMs) and pelleted by spinning at 1000 RPM for 5 minutes.

Cells were then lysed with 0.5 to 1 mL cold RIPA buffer in the presence of protease inhibitors (Sigma-Aldrich 11873580001) and phosphatase inhibitors (Sigma-Aldrich 4906837001). To increase protein yield and ensure lysis of nuclei, the lysate was subjected to additional mechanical disruption by passage 20 times through a 21-G needle. The mixture was shaken gently on ice for 15 minutes, and then centrifuged at >12000g for 10 to 15 minutes to pellet cell debris. The supernatant was transferred to a new tube, and the protein concentration was quantified using the BCA assay kit (Pierce).

LV tissue from mouse/human (~2×2mm piece) was lysed in 200 µL RIPA containing protease and phosphatase inhibitors as described for cells, and subsequently homogenized in TissueLyser (Qiagen) for 5 minutes at 25 Hz. Homogenized tissue was spun at 14 000g for 15 minutes to pellet cell debris. The supernatant was transferred to a new tube, and the protein concentration was quantified using the BCA assay kit (Pierce).

Coimmunoprecipitation

HEK293T cells, grown to confluence in a 10-cm tissue culture dish, were transfected with 15 µg total plasmid DNA (human ALPK3-FLAG: Origene RC220076, FLAG-FOXI3: Addgene Plasmid 153128, MYOM1 (myomesin 1)–HA (hemaglutinin): GenScript OHu 15548, or MYOM2 (myomesin 2, also called M-protein)–HA: GenScript Ohu 15548C) using Lipofectamine 3000 (Invitrogen L3000001) per the manufacturer's protocol. FLAG-IP was performed using anti-FLAG M2 magnetic beads per the manufacturer's protocol (Sigma-Aldrich M8823) and eluted with SDS-PAGE sample buffer for analysis by Western blot.

Western Blotting

Protein lysates were loaded and resolved under denaturing conditions on a NuPAGE 3% to 8% Tris-Acetate gel or NuPAGE 4% to 20% Tris-Glycine gel. Lysate was transferred to a PVDF membrane overnight at 40 mA at 4°C. Skim milk at 5% in 1× TBST buffer was used as a blocking agent. Primary antibodies used for Western blotting include mouse anti-FLAG 1:1000 (Sigma-Aldrich F1804), rabbit anti-HA 1:1000 (CST C29F4), rabbit anti-MYOM1 1:1000 (Abcam ab201228), mouse anti-cardiac troponin T 1:500 (Abcam ab8295), rabbit anti-MYOM2 1:500 (Abcam ab93915), rabbit anti-TUBB 1:1000 (Abcam ab6046), mouse anti-MuRF1 (muscle RING-finger protein 1) 1:1000 (Santa Cruz sc-398608), and rabbit anti-CAPN3 (calpain 3) 1:1000 (Proteintech 104-92-1-AP). Blots were blocked for at least 30 minutes at room temperature before addition to primary antibodies, incubated at 4°C overnight, and washed 3× with TBST before addition of mouse or rabbit secondary antibodies (Abcam ab97023, ab205718). Secondary antibodies were applied for 1 to 2 hours at 1:5000, washed 3× with TBST, and detected using Clarity Western ECL chemiluminescent substrates per the manufacturer's protocol (Bio-Rad 1705060).

Tandem-Mass-Tag Proteomics and Phosphoproteomics

Protein extracts were prepared and subjected to streamlined tandem-mass-tag quantitative (phospho)proteome profiling using synchronous precursor selection-MS3 as described previously.[25] For experiments with hiPSC-CMs, multiple tandem-mass-tag experiments were run: 1 phosphoproteomics 11-plex (WT n=4, *ALPK3*$^{dIC/dIC}$ n=4, *ALPK3*$^{ns/del}$ n=3) from which both phosphopeptide and protein abundances were determined, and another 10-plex with additional differentiations of hiPSC-CMs (WT n=4, *ALPK3*$^{dIC/dIC}$ n=3, *ALPK3*$^{ns/del}$ n=3) from which protein abundances were determined and normalized to WT levels for comparison across both 10- and 11-plex experiments (5587 total proteins, 3712 phosphopeptides quantitated in both experiments). To later validate results, another phosphoproteomics 12-plex with additional cell lines was performed (WT n=4, *ALPK3*$^{sIC/sIC}$ n=4, *ALPK3*$^{del/del}$ validation n=4; 7970 total proteins, 5818 phosphopeptides).

Briefly, cells/tissues were lysed, after which cysteine bonds were reduced with 5 mM tris(2-carboxyethyl)phosphine and alkylated with 10 mM iodoacetamide that was quenched with 10 mM dithiothreitol. A total of 100 µg protein per sample methanol-chloroform precipitated to extract proteins, which were subsequently digested using Lys-C (Wako) overnight followed by digestion with trypsin (Thermo Fisher Scientific) for 6 hours. The resulting peptides were labeled with tandem-mass-tag isobaric tags. To check mixing ratios, 2 µg of each sample was pooled, desalted, and analyzed by mass spectrometry. Using normalization factors calculated from this "label check," samples were mixed 1:1 across all channels, and a single desalting step was performed using a 100-mg Sep-Pak solid-phase extraction column (Waters). The dried, mixed, and desalted sample was subjected to centrifugation-based phosphopeptide enrichment using the Pierce High-Select Fe-NTA phosphopeptide enrichment kit (Thermo Fisher Scientific). Enriched phosphopeptides were desalted for SPS-MS3 analysis. The flow-through unbound fraction and washes from this enrichment were combined, desalted, and fractionated by basic pH reverse-phase high-performance liquid chromatography. The resulting fractions were desalted by StageTip and analyzed by liquid chromatography–tandem mass spectrometry. Mass-spectrometric data were collected on an Orbitrap Fusion mass spectrometer in line with a Proxeon NanoLC-1200 ultra-high performance chromatography. Database searching and reporter-ion quantification were performed using an in-house SEQUEST-based pipeline. Each protein was scaled such that the summed signal to noise for that protein across all channels was 100, thereby generating a relative abundance measurement.

RNA Sequencing

hiPSC-CMs and mouse LV tissue were lysed in Trizol Reagent (Life Technologies); mouse tissue was subjected to additional 2 minutes of mechanical bead homogenization using a TissueLyser (Qiagen). RNA sequencing was performed as previously described.[26] Briefly, RNA was isolated by chloroform:isopropyl alcohol extraction. RNA quality was assessed using the RNA integrity number and quantity were assessed on the TapeStation 2200 (Agilent). Two rounds of mRNA purification were performed on total RNA (1 µg) using Dynabeads mRNA DIRECT Kit (Invitrogen). The Superscript III First-Strand Synthesis System (Invitrogen) was used to generate double-stranded cDNA. cDNA libraries were constructed using the Nextera XT DNA Library Preparation Kit (Illumina). Libraries were sequenced on the Illumina NextSeq500 platform. A total of 75-bp paired-end reads were aligned to the human reference genome hg38 using Spliced Transcripts Alignment to a Reference (STAR). Raw reads were normalized to the total number of reads per kilobase of transcript per million. For analysis of human LV tissues, nuclei were isolated, and single nuclear RNA sequencing was performed as described elsewhere.[16,27]

Mouse Echocardiography

Cardiac function was evaluated by a skilled echocardiographer who was blinded to mouse genotypes. Newborn pups were not anesthetized, whereas older mice were anesthetized under isoflurane vaporizer (VetEquip). Each limb was placed

on the ECG leads on a Vevo Mouse Handling Table (FujiFilm VisualSonics) to maintain body temperature at 37°C during the study. Chest hair was removed with depilatory cream to obtain clear images. Anesthesia was terminated after a mouse was properly positioned for imaging, and all measurements were performed with a heart rate between 300 and 550 beats per minute. Two-dimensional and M-mode images of the LV (parasternal long axis and short axis) were obtained. Measurements were averaged from M-mode tracings of 3 consecutive heartbeats including LV end-diastolic dimension (LVEDD), end-systolic dimension (LVESD), LV posterior wall thickness, and interventricular septal thickness. LV fractional shortening (FS) was calculated by the following equation: FS = 100 × [(LVEDD – LVESD)/LVEDD].

Immunofluorescence

hiPSC-CMs were replated onto Matrigel-coated glass-bottom imaging-optimized 12-well plates (Mat-Tek).[28] hiPSC-CMs were cultured in RPMI B27 plus insulin containing 5 μM ROCK inhibitor and 20% FBS for 2 days after replating, after which they were cultured in RPMI B27 plus insulin for 1 week before imaging analysis. For transient transfection experiments, replated hiPSC-CMs were transfected with 1 μg total plasmid DNA encoding human ALPK3-FLAG (Origene RC220076), MYOM1-HA (GenScript OHu 15548), or MYOM2-HA (GenScript OHu 15548C) using Lipofectamine 3000 (Invitrogen L3000001) per the manufacturer's protocol and incubated for 72 hours before imaging.

Murine cardiomyocytes were isolated from 7- to 9-week-old mice by rapid excision of the heart and aortic cannulation on a Langendorff apparatus as described previously.[29] Isolated cardiomyocytes were plated in glass-bottom imaging-optimized 12-well plates (Mat-Tek) that had been precoated with laminin at a concentration of 10 μg/mL in PBS.[29]

hiPSC-CMs or murine cardiomyocytes were fixed with 4% paraformaldehyde (10 min), rinsed with PBS (5 minutes 3×), permeabilized with 0.2% Triton-100 (5 minutes), rinsed with PBS 1×, and incubated overnight at 4°C in PBS with 3% BSA and primary antibody (mouse anti-FLAG M2 [Sigma-Aldrich F1804 1:1000]; rabbit anti-HA [Cell Signaling Technologies C29F4 1:000], rabbit MYOM2 [Abcam ab93915 1:100], and mouse MYOM1 0.3 μg/mL [distributed as mMaC myomesin B4; Developmental Studies Hybridoma Bank]). Wells were rinsed with PBS (5 minutes 3×), and samples were incubated with respective secondary antibodies (Abcam ab150080, ab150116, abcam 150077, abcam ab150113) at a dilution of 1:1000 for 2 hours at room temperature before imaging with a spinning disk confocal microscope (Yokogawa CSU-W1 Spinning Disk on Nikon T1). Images were analyzed using Fiji software.

Electron Microscopy

Mice were euthanized, and LV tissue was isolated under a dissecting microscope. LV tissue was cut into small pieces (1- to 2-mm cubes) and perfused in 1% glutaraldehyde/3% paraformaldehyde in cardioplegic buffer (5% dextrose, 30 mmol/L KCl in PBS).[30] After fixation, the tissue was washed in 0.1 M cacodylate buffer and postfixed with 1% osmiumtetroxide (OsO_4)/1.5% potassium ferrocyanide ($C_6FeK_4N_6$) for 1 hour, washed in water 3×, and incubated in 1% aqueous uranyl acetate for 1 hour followed by 2 washes in water and subsequent dehydration in grades of alcohol (10 min each, 50%, 70%, 90%, 2× 10 minutes 100%). The samples were then put in propyleneoxide for 1 hour and infiltrated ON in a 1:1 mixture of propyleneoxide and TAAB Epon (Marivac Canada Inc, St Laurent, Canada). The following day, the samples were embedded in TAAB Epon and polymerized at 60°C for 48 hours. Ultrathin sections (about 80 nm) were cut on a Reichert Ultracut-S microtome, picked up onto copper grids, stained with lead citrate, and examined in a JEOL 1200EX Transmission electron microscope or a TecnaiG² Spirit BioTWIN. Images were recorded with an AMT 2k CCD camera and saved as TIFF files.

Quantification and Statistical Analysis

All statistical comparisons and sample sizes are included in the figures and figure legends. Unpaired 2-sided *t* tests were used to determine *P* values for all proteomics/phosphoproteomics analysis. DESeq2 was used to analyze RNA sequencing data and determine differentially expressed (DE) RNAs.[31] No samples were excluded. Data were visualized and graphics were generated using the RStudio programming environment, Prism 8 (GraphPad), and Biorender. Nonlinear lines of best fit for mouse echocardiography parameters of cardiac function were fitted using Prism 8. In experiments using cell lines, "n" indicates independent differentiations into hiPSC-CMs. In experiments using mouse tissue, "n" refers to the number of animals.

RESULTS

Structure and Conservation of the ALPK3 α-Kinase Domain

We examined the relative conservation of the ALPK3 α-kinase domain by sequence alignment relative to the 5 other human α-kinase protein domains (Figure 1B). This analysis identified 16 amino acid residues that are entirely conserved among all human α-kinase family members (Figure 1B, red). Four additional residues are conserved in all α-kinases except ALPK3 (Figure 1B, green). Moreover, these 4 residues are conserved in all α-kinase orthologs (mouse, chicken, frog, zebrafish, and the evolutionarily distant slime mold *Dictyostelium discoideum*) *except* for the ALPK3 orthologs (Figure 1B, Figure S1). We denote these 4 as ALPK3-specific nonconserved residues.

Because the structure of ALPK3 is unsolved, we mapped the corresponding ALPK3 residues onto the TRPM7 α-kinase domain by sequence homology (Figure 1C, Table S1).[10,11] The sixteen conserved residues were found to reside within the P-loop, interlobe cleft region, which positions ATP, and C-terminal lobe region, which chelates zinc and stabilizes the tertiary domain structure[10,11] (Figure 1C, Table S1). All 4 ALPK3-specific nonconserved residues were contained in the interlobe cleft, 2 of which (S1731, A1776) occupied positions involved in positioning ATP, and 1 of which (S1800) is predicted be involved in substrate binding.[10,12] The

ORIGINAL RESEARCH ARTICLE

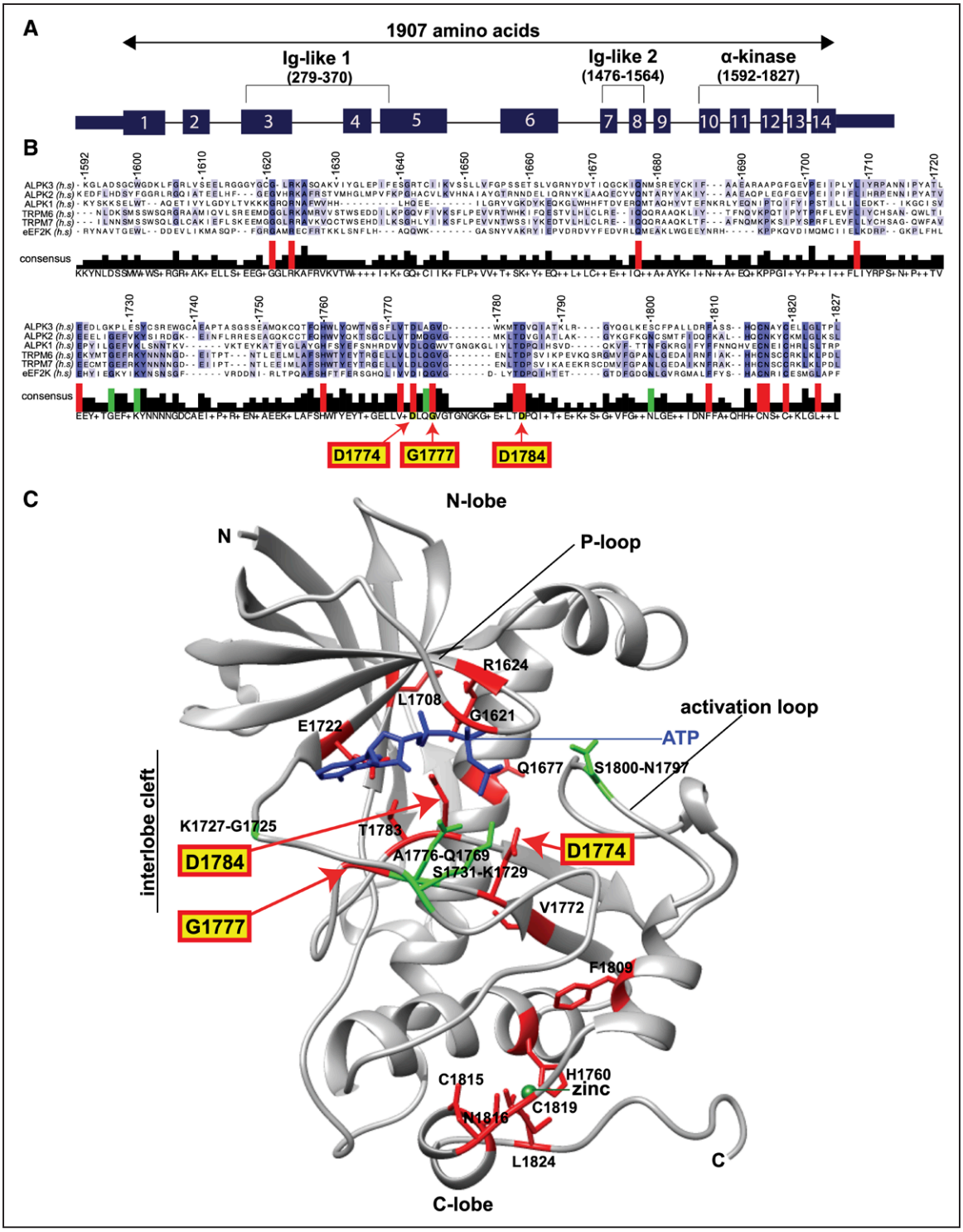

Figure 1. Sequence alignment of all α-kinase domains shows 4 nonconserved interlobe cleft residues in ALPK3.
A, The *ALPK3* gene contains 14 exons that encode 3 protein domains and 1907 amino acids (positions indicated in parentheses). **B**, Sequence alignment of 6 human α-kinase domains (numbered by amino acid position in ALPK3) identifies 16 residues (red) that are uniformly conserved. Four residues (green) are conserved in all α-kinases (including 26 α-kinase orthologs) *except* ALPK3 (denoted ALPK3-specific nonconserved residues; see also Figure S1). The positions of 3 conserved residues edited by CRISPR/Cas9 (G1777E, D1784A, D1774A) are indicated with red arrows. **C**, The positions of conserved and ALPK3-specific nonconserved residues are indicated with colors and symbols as in **B** by homology mapping to the TRPM7 α-kinase domain.[10,11] Hyphenated residues denote amino acids in ALPK3 and TRPM7, respectively. Three of the 4 ALPK3-specific nonconserved residues are predicted to position ATP and bind substrate (see also Table S1). ATP (blue), zinc (green). ALPK3 indicates α-kinase 3; C-lobe, C-terminal lobe; and N-lobe, N-terminal lobe.

absence of these 4 residues in ALPK3 that are otherwise entirely conserved among all α-kinase family members prompted the hypothesis that ALPK3 might lack catalytic activity.

Characterization of *ALPK3* Mutant hiPSCs and Differentiation Into hiPSC-CMs

To investigate the putative catalytic activity of ALPK3, we used CRISPR/Cas9 gene editing to create isogenic hiPSCs carrying either WT or mutated *ALPK3* alleles and then differentiated these into hiPSC-CMs. These hiPSCs also contained an N-terminal eGFP tag on TTN, a protein spanning the Z-disc to M-band of sarcomeres, which enables monitoring of sarcomere contraction in hiPSC-CMs.[15,24]

The *ALPK3*$^{ins/del}$ hiPSC line carries compound frameshift variants (Table). A single base insertion (c.2442_2443insA) causes a missense residue at position p.815 and results in a premature stop codon; the other allele contains a deletion (c.2428_2458del31) that excises residues p.809-819 and results in a premature stop codon. The *ALPK3*$^{G1777ED1784A/G1777ED1784A}$ hiPSC line (henceforth denoted as "dual interlobe cleft" by *ALPK3*$^{dIC/dIC}$) carries homozygous dinucleotide (c.5330-5331GG>AA) and mononucleotide (c.5351A>C) substitutions. These substitutions alter 2 conserved residues that reside in the kinase domain interlobe cleft in close proximity to the ATP binding pocket (G1777E and D1784A; Figure 1C, Table) and are predicted to alter the conformation of the α-kinase domain.

We also produced 2 additional *ALPK3* mutant lines to further study and validate results (Table). The *ALPK3*$^{del/del}$ hiPSC line carries compound frameshift variants. One allele contains a 20-base deletion (c.5306_5325del20) that produces a missense residue at p.1769, excises residues p.1770-1775, and causes a premature stop codon; the other allele contains an 11-base deletion (c.5310_5320del11) that produces a missense residue at p.1770, excises residues p.1771-1773, and causes a premature stop codon. The *ALPK3*$^{D1774A/D1774A}$ hiPSC line (henceforth denoted as "single interlobe cleft" by *ALPK3*$^{sIC/sIC}$) carries homozygous mononucleotide (c.5321A>C) substitutions that alter a conserved aspartate residue (predicted to be the essential "catalytic" aspartate) in the kinase domain (D1774A; Figure 1C, Table). All hiPSC lines were subcloned, sequence-validated (Figure S2A through S2D), and ploidy-confirmed across all chromosomes (see Methods).

Table. Isogenic hiPSC Models With Biallelic *ALPK3* Mutations

ALPK3 mutant hiPSC line	*ALPK3* cDNA variants	Variant class	ALPK3 protein level
ALPK3$^{ins/del}$	c.2442_2443insA c.2428_2458del31	Frameshift Frameshift	<5% WT
ALPK3$^{dIC/dIC}$	c.5330_5331GG>AA (homozygous) c.5351A>C (homozygous)	Missense, G1777E Missense, D1784A	~2× WT
ALPK3$^{del/del}$	c.5306_5325del20 c.5310_5320del11	Frameshift Frameshift	~39% WT
ALPK3$^{sIC/sIC}$	c.5321A>C (homozygous)	Missense, D1774A	~1× WT

See Figure S1 for sequence validation and Figure S2F and S2H for ALPK3 protein-level quantitation. ALPK3 indicates α-kinase 3; dIC, dual interlobe cleft variant; hiPSC, human induced pluripotent stem cell; sIC, single interlobe cleft variant; and WT, wild type.

Because previous reports suggested that *ALPK3* expression might affect cardiomyocyte maturity,[13] we compared the differentiation potential of WT and *ALPK3*$^{ins/del}$ hiPSCs. Both WT and *ALPK3*$^{ins/del}$ hiPSC differentiations produced beating hiPSC-CMs with similar contractile performance (Methods, see below). Principal component analyses of RNA sequencing at 4 time points during the 30-day differentiation protocol confirmed comparable maturation efficiency of WT and *ALPK3*$^{ins/del}$ hiPSC-CMs (Figure S2E), with similar transcript expression of prototypic cardiomyocyte genes by day 30 (Supplemental Data S1).

To investigate the putative kinase activity of ALPK3, multiple independent batches of WT (n=8), *ALPK3*$^{dIC/dIC}$ (n=4), and *ALPK3*$^{ins/del}$ (n=7) hiPSCs were differentiated into hiPSC-CMs, and the resultant protein extracts were analyzed by multiplexed mass spectrometry using tandem-mass-tag phosphoproteomics (see Methods) with 3714 phosphopeptides (Supplemental Data S2) and 5587 proteins (Supplemental Data S3) quantified in all samples. *ALPK3*$^{ins/del}$ hiPSC-CMs had profoundly reduced ALPK3 protein expression (<5% WT), with reduced levels of ALPK3 peptides across the entire length of the protein (Figure S2F). Unexpectedly, *ALPK3*$^{dIC/dIC}$ hiPSC-CMs had approximately twice the ALPK3 protein levels compared with WT (Figure S2F), although there was no increase in *ALPK3* transcript levels, as assessed by RNA sequencing (Figure S2G). We suggest that *ALPK3*$^{dIC/dIC}$ hiPSCs, which contain substitutions at 2 conserved amino acid residues, may alter the kinase domain conformation and inhibit interactions with ubiquitinases or other degradatory machinery, and thereby increase protein levels. *ALPK3*$^{sIC/sIC}$ hiPSC-CMs had comparable levels of ALPK3 protein as WT (Figure S2H). *ALPK3*$^{del/del}$ hiPSC-CMs had reduced ALPK3 protein expression (~39% WT), indicating that these cells produce a truncated ALPK3 protein with reduced stability (Figure S2H).

ALPK3 Is a Pseudokinase That Lacks Significant Catalytic Activity

To investigate the putative catalytic activity of ALPK3, we initially compared the phosphoproteomes of

ORIGINAL RESEARCH ARTICLE

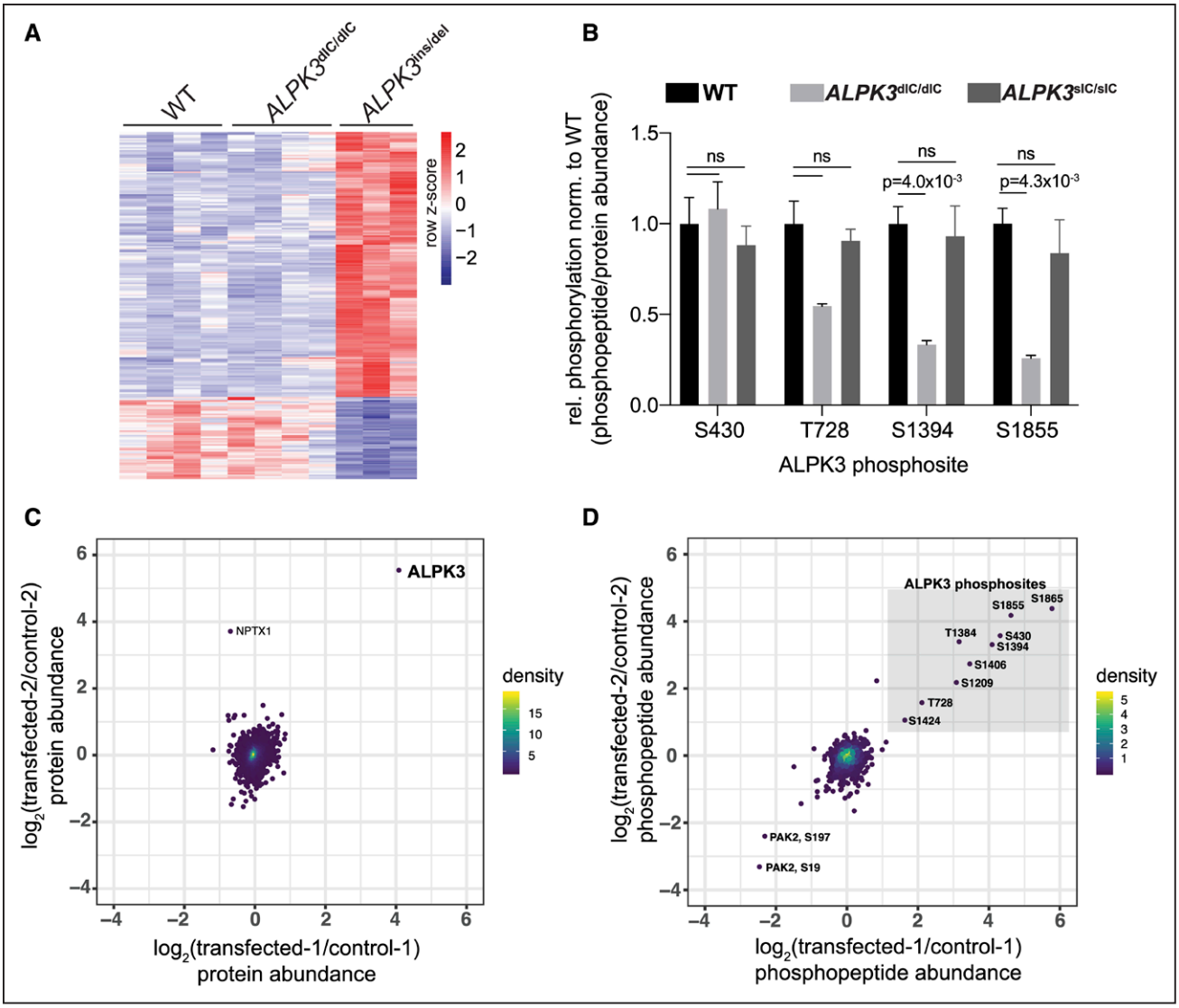

Figure 2. Phosphoproteomic analyses of ALPK3 kinase domain inhibition and overexpression fail to detect ALPK3 catalytic activity.

A, Heatmap of differentially phosphorylated (DP) sites in *ALPK3*-mutant hiPSC-CMs versus WT determined by tandem-mass-tag phosphoproteomics. A total of 3714 phosphosites were identified on 1630 unique proteins (see also Supplemental Data S2). Columns represent independent cultures of each hiPSC cell genotype (see Methods). In comparison with isogenic WT, *ALPK3*$^{ns/del}$ hiPSC-CMs have 225 DP sites (171 up, 54 down), and *ALPK3*$^{dIC/dIC}$ hiPSC-CMs have 3 DP sites (1 up, 2 down). DP criteria: $|\log_2$-fold change$|>0.67$ and unadjusted *P* value <0.01, 2o-sided *t*-test (WT n=4; *ALPK3*$^{dIC/dIC}$ n=4; *ALPK3*$^{ns/del}$ n=3). **B**, Four phosphosites are detected on the ALPK3 protein. The only 2 DP sites with reduced phosphorylation relative to protein expression in *ALPK3*$^{dIC/dIC}$ hiPSC-CMs occur on ALPK3 S1394 and ALPK3 S1855; these sites are not affected in *ALPK3*$^{sIC/sIC}$ hiPSC-CMs (n=4). **C**, Log-log plot of protein abundance in HEK293T cells transfected with ALPK3 versus control cells. Each point represents a single protein (n=6596). The level of ALPK3 in transfected samples is highly increased relative to controls (see also Supplemental Data S4; ALPK3 transfected n=2; control n=2). **D**, Log-log plot of phosphopeptide abundance (n=1158 phosphopeptides) in HEK293T cells transfected with ALPK3 versus control cells. The levels of 9 ALPK3 phosphopeptides (gray box, phosphorylated residues denoted) were highly increased in ALPK3-transfected versus control cells, whereas all other phosphopeptides were minimally affected (see also Supplemental Data S4; ALPK3-transfected n=2; control n=2). For **C** and **D**, point density is indicated by color scale as shown. ALPK3 indicates α-kinase 3; dIC, dual interlobe cleft variant; hiPSC, human induced pluripotent stem cell; hiPSC-CM, hiPSC-derived cardiomyocyte; and WT, wild type.

WT, *ALPK3*$^{dICd/IC}$, and *ALPK3*$^{ns/del}$ hiPSC-CMs. We hypothesized that if ALPK3 were a catalytically active kinase, its substrates would have depleted phosphorylation in both the *ALPK3*$^{dIC/dIC}$ and *ALPK3*$^{ns/del}$ lines.

Analyses of 3714 phosphopeptides revealed that the patterns of phosphorylation of *ALPK3*$^{dIC/dIC}$ and WT hiPSC-CMs were nearly identical (Figure 2A). Only 2 sites had significantly depleted phosphorylation in *ALPK3*$^{dIC/dIC}$ hiPSC-CMs relative to WT, both of which resided within the ALPK3 protein itself (ALPK3 residues S1384 and S1855) (Figure 2B, Supplemental Data S2). Although *ALPK3*$^{ns/del}$ hiPSC-CMs had many more differentially phosphorylated sites (n=225), ~75% of these had *increased* phosphorylation relative to WT (Figure 2A,

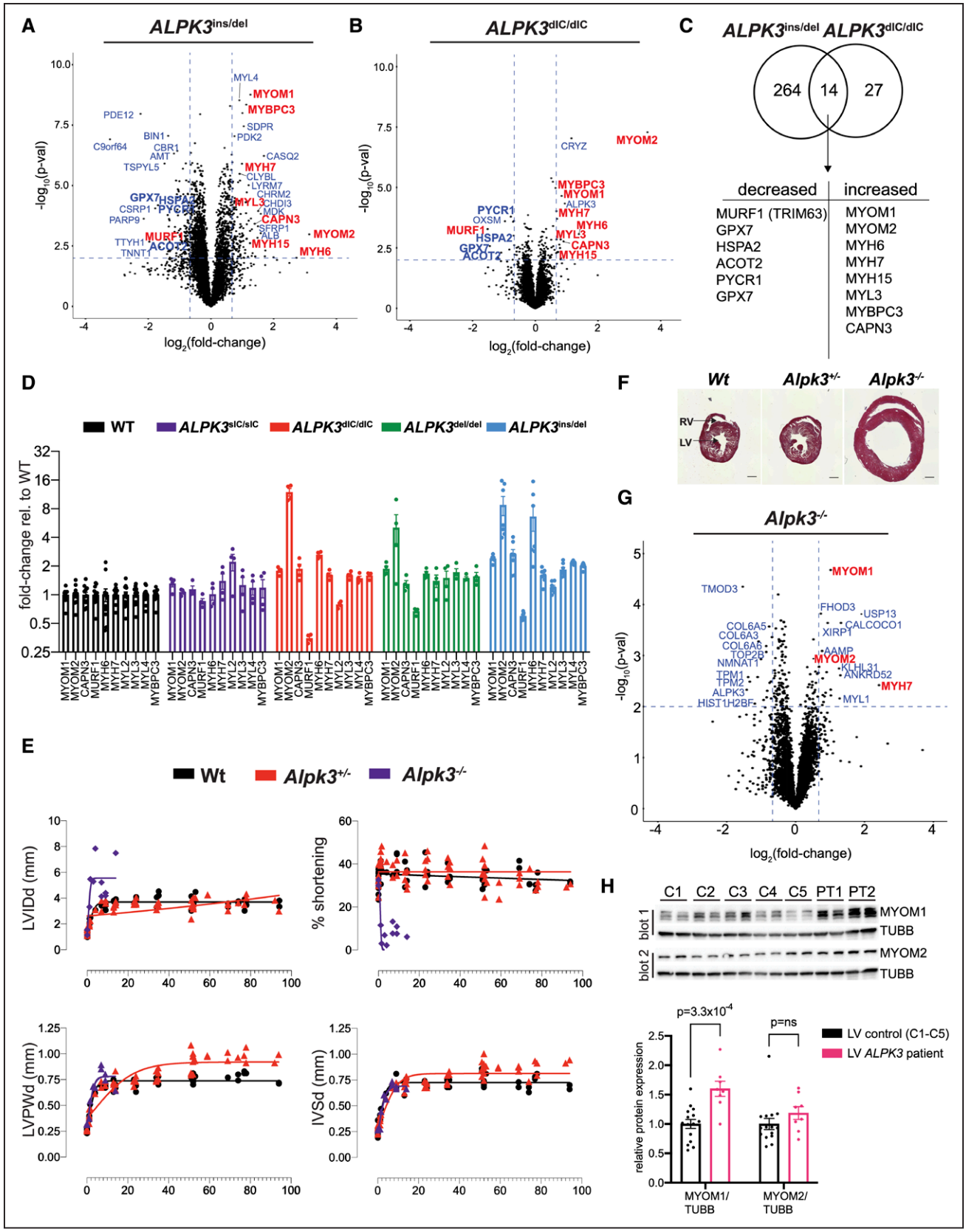

Figure 3. *ALPK3* variants dysregulate myomesin and thick filament proteins in hiPSC-CMs, mice, and human tissues.
A and **B**, Volcano plots of protein expression in *ALPK3*$^{ins/del}$ hiPSC-CMs (n=7) versus WT (n=8) and *ALPK3*$^{dIC/dIC}$ hiPSC-CMs (n=4) versus WT (n=5587 total proteins). Dashed lines indicate cutoffs for differential expression: $|\log_2\text{-fold change}| \geq 0.67$ and unadjusted *t*-test *P* value <0.01. Sarcomere M-band and thick filament proteins are highlighted in red (see also Supplemental Data S3). (*Continued*)

Figure 3 Continued. C, Overlap of proteins with altered expression in *ALPK3*$^{ns/del}$ and *ALPK3*$^{dIC/dIC}$ hiPSC-CMs. **D**, Fold-change of M-band and thick filament proteins in *ALPK3*$^{sIC/sIC}$ (n=4), *ALPK3*$^{dIC/dIC}$ (n=4), *ALPK3*$^{del/del}$ (n=4), and *ALPK3*$^{ns/del}$ (n=7) hiPSC-CMs relative to WT (n=12). **E**, Serial echocardiographic measurements (*x* axis, age in weeks) of WT and *Alpk3* mutant mice. No measurements are reported in *Alpk3*$^{-/-}$ mice after 14 weeks because of early lethality. **F**, Transverse cardiac sections showing ventricular enlargement of *Alpk3*$^{-/-}$ heart at 14 weeks (Masson trichrome stain, scale bar=1 mm). **G**, Volcano plot of protein expression in LV tissues harvested at postnatal day 8 from *Alpk3*$^{-/-}$ vs WT mice (n=5678 total proteins; see also Supplemental Data S3). Proteins are identified by their human homologues. Dashed lines and labels are as in **A** and **B** (WT, n=4; *Alpk3*$^{+/-}$, n=3, *Alpk3*$^{-/-}$, n=3). **H**, **Upper**, Western blotting analysis of LV tissues from human subjects with compound heterozygous variants in *ALPK3* (PT1-PT2) compared with adult healthy control tissues (C1-C5) probed with (blot 1) myomesin-1 (MYOM1, blot 1), tubulin (TUBB), and myomesin-2 (MYOM2, blot 2) antibodies (n=3 technical replicates per sample; see also Table S2). **Lower**, Western blotting quantification of MYOM1 and MYOM2 expression in human ALPK3-deficient subjects and ALPK3-normal subjects (normalized to TUBB levels). Data are mean±SEM. ALPK3 indicates α-kinase 3; dIC, dual interlobe cleft variant; hiPSC-CM, human induced pluripotent stem cell–derived cardiomyocyte; IVSd, interventricular septal thickness at end-diastole; LV, left ventricle; LVIDd, LV internal dimension at end diastole; LVPWd, LV posterior wall thickness at end-diastole; sIC, single interlobe cleft variant; and WT, wild type.

Supplemental Data S2), indicating that these did not represent direct ALPK3 substrates.

Additional phosphoproteomic investigations of *ALPK3*$^{sIC/sIC}$ hiPSC-CMs confirmed that this line had few differences in phosphorylation relative to WT (n=19 differentially phosphorylated peptides versus expected ~50 false positives (calculated as 0.01×5009 total phosphopeptides), and no differences in phosphorylation on sites residing within the ALPK3 protein relative to WT (Figure 2B, Supplemental Data S2). These findings suggested that the altered phosphorylation on ALPK3 S1384 and S1855 in *ALPK3*$^{dIC/dIC}$ hiPSC-CMs is likely a result of the altered conformation of the kinase domain in this mutant rather than loss of any autophosphorylative activity. Analyses of differentially phosphorylated sites in *ALPK3*$^{del/del}$ hiPSC-CMs showed few differentially phosphorylated sites relative to *ALPK3*$^{ns/del}$ hiPSC-CMs (n=15 versus 225, Supplemental Data S2). These findings suggest that *ALPK3*$^{del/del}$ hiPSC-CMs produce an unstable truncated ALPK3 protein (Figure S2H) that still may be able to participate in noncatalytic (ie, scaffolding) roles, unlike ALPK3$^{ins/del}$ hiPSC-CMs, which have nearly complete loss of ALPK3 protein expression (Figure S2F). On the basis of these data and the paucity of differentially phosphorylated sites in both *ALPK3*$^{dIC/dIC}$ and *ALPK3*$^{sIC/sIC}$ hiPSC-CMs, we inferred that ALPK3 lacks significant catalytic activity.

We confirmed the absence of ALPK3 catalytic activity by transiently overexpressing *ALPK3* in HEK293T cells, and comparing the phosphoproteomes (1158 unique phosphopeptides, 6596 unique proteins) of transfected and control cells (Supplemental Data S4). ALPK3 protein expression was >16-fold higher in transfected versus control cells (Figure 2C, Figure S3A and S3B). Only 9 phosphopeptides had reproducibly increased abundance in transfected versus control cells, and all were within ALPK3 (Figure 2D). The increased abundance of these phosphopeptides is consistent with increased ALPK3 protein abundance in the transfected lines; ALPK3 overexpression did not increase the phosphorylation of any of the other 1000+ phosphosites across the HEK293T phosphoproteome, supporting the conclusion that ALPK3 is a pseudokinase.

ALPK3 Loss-of-Function Dysregulates Myomesins and Associated Thick Filament Proteins in hiPSC-CMs

To explore other possible functions of ALPK3, we first compared the proteomes of *ALPK3*$^{ns/del}$ and WT hiPSC-CMs (n=5587 total proteins). *ALPK3*$^{ns/del}$ hiPSC-CMs had 264 DE proteins and *ALPK3*$^{dIC/dIC}$ hiPSC-CMs had 27 DE proteins relative to WT (Figure 3A and 3B, Supplemental Data S3). Fourteen DE proteins were shared by both *ALPK3*$^{ns/del}$ and *ALPK3*$^{dIC/dIC}$ hiPSC-CMs, which is significantly more than expected by chance (P=2.3×10^{-12}, hypergeometric test), indicating that the *ALPK3*$^{dIC/dIC}$ variant had partial loss-of-function effects (Figure 3C).

Several of the shared DE proteins were components of the M-band, a central transverse zone that demarcates half a sarcomere[32] (Figure 3A through 3C). The major constituents of the M-band are myomesin proteins that cross-link myosins and buffer forces generated by opposing thick filaments during sarcomere contraction by multiple extensible α-helical domains.[33,34] The levels of both MYOM1 and MYOM2 were increased in *ALPK3*$^{ns/del}$ and *ALPK3*$^{dIC/dIC}$ hiPSC-CMs, as were the levels of thick filament proteins bound by myomesins, including MYH6 (α-myosin heavy chain), MYH7 (β-myosin heavy chain), MYL3 (myosin essential light chain), and MYBPC3 (myosin-binding protein c; Figure 3A through 3C). Because myosin heavy chain isoforms and myomesins share 93% and 43% sequence identity, respectively, the abundances of these proteins were recalculated after restricting the analysis to include only uniquely mapping peptides, which confirmed that both myosin heavy chain proteins (MYH6, MYH7) and myomesin proteins (MYOM1, MYOM2) were increased in *ALPK3*$^{ns/del}$ and *ALPK3*$^{dIC/dIC}$ hiPSC-CMs relative to WT (Figure S5B, Supplemental Data S3). Two shared DE proteins (MuRF1, decreased; CAPN3, increased) also localize to the M-band and are known to regulate sarcomere protein turnover.[35–38]

To further study and validate these changes, we performed additional phosphoproteomic studies of *ALPK3*$^{sIC/sIC}$ and *ALPK3*$^{del/del}$ hiPSC-CMs (Supplemental Data S2 and S3). *ALPK3*$^{del/del}$ hiPSC-CMs had similar but less severe changes in M-band and thick filament proteins levels as *ALPK3*$^{ns/del}$ hiPSC-CMs, including increased

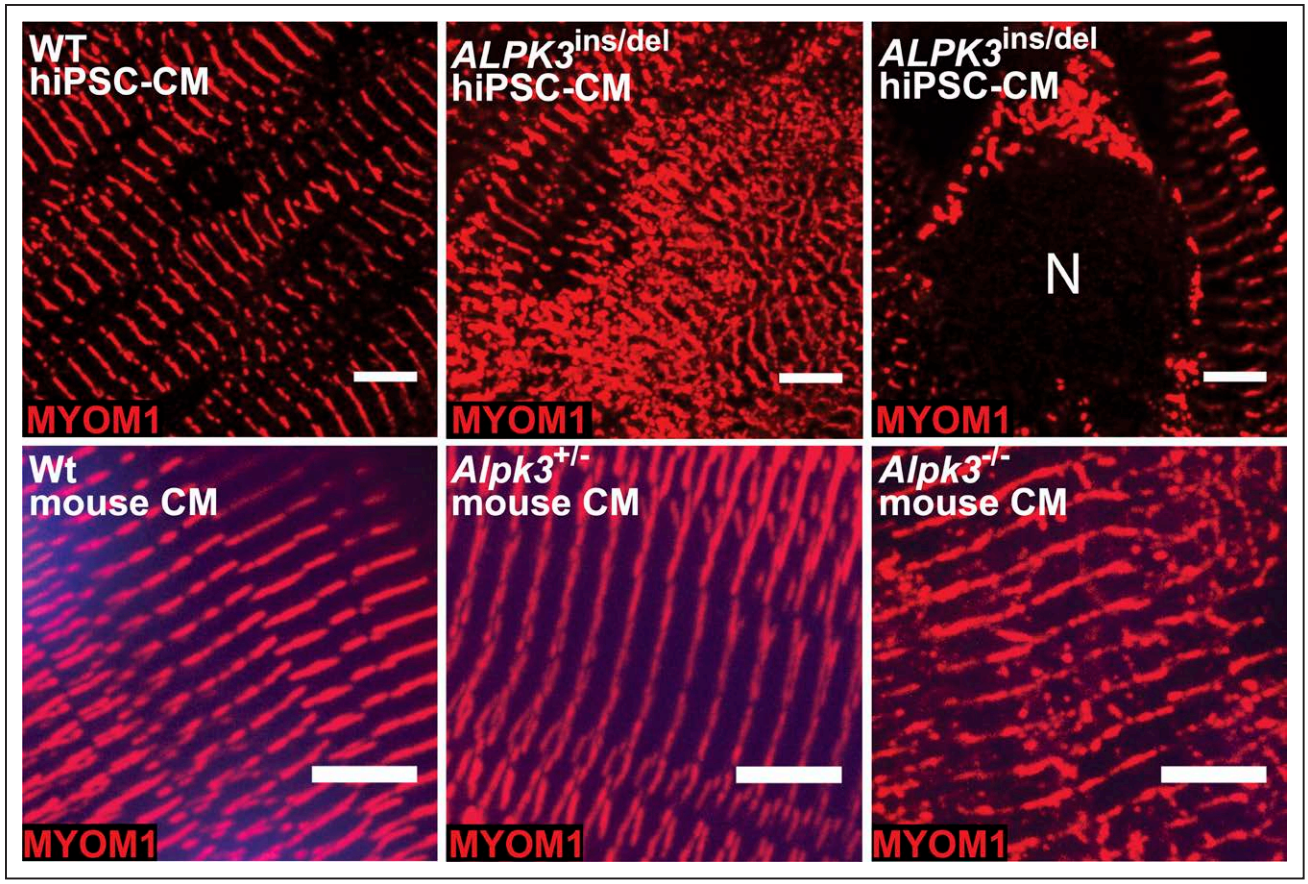

Figure 4. Confocal micrographs of WT and *ALPK3*-deficient hiPSC-CMs and murine cardiomyocytes stained with MYOM1 antibody (red) demonstrate myomesin-1 accumulation in mutant cells.
Top, MYOM1 accumulates outside the M-band and around the nucleus (N) in *ALPK3*$^{ns/del}$ hiPSC-CMs versus WT. Scale bar=5 μm**. Bottom**, Myom1 accumulates outside the M-band in *Alpk3*$^{-/-}$ mouse cardiomyocytes (left ventricular cardiomyocytes isolated from mice age 7–9 weeks). Scale bar=5 μm (see also Figure S7 for confocal micrographs of entire cardiomyocytes). ALPK3 indicates α-kinase 3; hiPSC-CM, human induced pluripotent stem cell–derived cardiomyocyte; MYOM1, myomesin-1; and WT, wild type.

MYOM1, MYOM2, and CAPN3 and reduced MuRF1 levels (Figure 3D). Unlike *ALPK3*$^{dIC/dIC}$, *ALPK3*$^{ns/del}$, and *ALPK3*$^{del/del}$ hiPSC-CMs, the *ALPK3*$^{sIC/sIC}$ hiPSC-CMs did *not* show changes in myomesin and thick filament protein levels (Figure 3D), further supporting a noncatalytic role of ALPK3 in regulating the M-band and thick filament proteins.

High-throughput analyses of the sarcomere contractility (>40 000 total tracked sarcomeres per cell line) assessed using the SarcTrack algorithm[24] did not detect significant differences between WT, *ALPK3*$^{ns/del}$, and *ALPK3*$^{dIC/dIC}$ hiPSC-CMs (Figure S5A).

Alpk3 Deficiency in Mice Causes Cardiomyopathy and Dysregulates Myomesin and Associated Thick-Filament Proteins

Because we did not detect differences in sarcomere contractility between WT and *ALPK3* mutant hiPSC-CMs, which may reflect the absence of hemodynamic influences, we assessed the in vivo consequences of *ALPK3* variants by studying a mammalian model. A previous *Alpk3*$^{-/-}$ C57BL/6J mouse model[14] failed to recapitulate the rapidly progressive and often fatal neonatal disease that is observed in human patients.[3,6] We therefore acquired and studied an alternative model, C57BL/6N *Alpk3*$^{+/-}$ mice (MRC Harwell Institute), that was created by deleting a region encompassing exon 3 (Figure S4). Heterozygous matings produced *Alpk3*$^{-/-}$ mice at expected Mendelian ratios.

Serial longitudinal echocardiography beginning at postnatal day 0 showed that *Alpk3*$^{-/-}$ mice had normal cardiac function at birth but manifested a rapidly progressive cardiomyopathy in the first week of life that resulted in premature death (no survivors beyond 14 weeks). Longitudinal cardiac imaging showed that relative to WT, *Alpk3*$^{-/-}$ mice had increased LV cavity dimensions and severely diminished contractile function (Figure 3E and 3F, mean percent shortening age 1 to 14 weeks: *Alpk3*$^{-/-}$ (n=11)=7.7%; WT (n=22)=37.5%; $P=1.1\times10^{-9}$).

Alpk3$^{+/-}$ heterozygote mice had normal contractile function, fertility, and survival, but developed significant ventricular hypertrophy beyond 1 year of age, supporting the pathogenicity of *Alpk3* heterozygote variants in adult

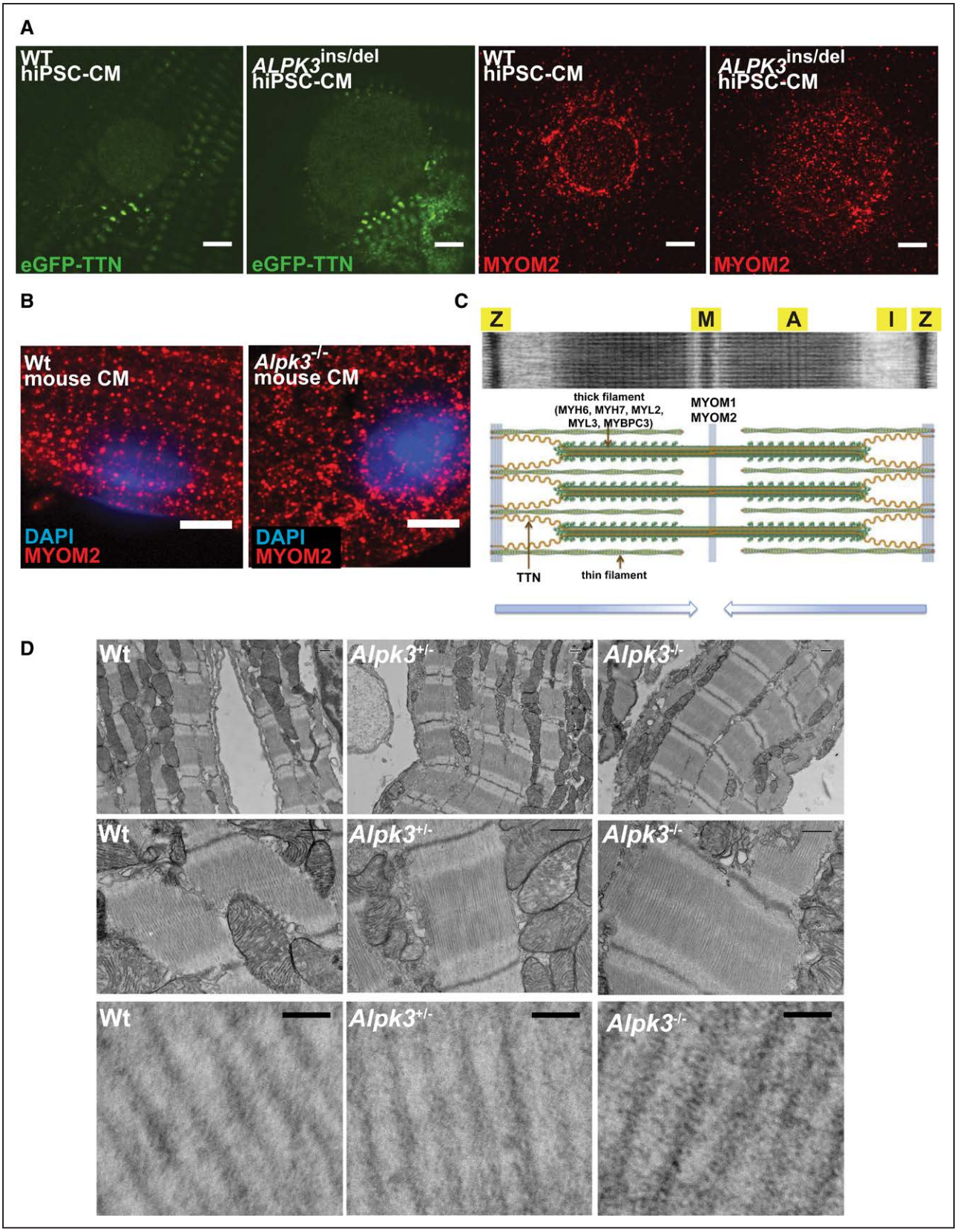

Figure 5. Confocal micrographs and electron microscopy demonstrate the effects of ALPK3 deficiency on the localization of myomesins and sarcomere structure in cardiomyocytes.

A, Confocal micrographs of WT and *ALPK3*$^{ins/del}$ hiPSC-CMs expressing eGFP-TTN (green), probed with MYOM2 antibody (red). **Left**, eGFP-TTN expression in WT and *ALPK3*$^{ins/del}$ nuclei is indistinguishable. **Right**, Prominent localization of myomesin-2 of the nuclear lamina in (*Continued*)

Figure 5 Continued. WT compared with diffuse staining across the nucleus in *ALPK3*$^{ns/del}$ CMs. Scale bar=5 µm. **B**, MYOM2 immunofluorescence is organized into striations at the M-band in WT murine LV cardiomyocytes, but scattered without striations in *Alpk3*$^{-/-}$ murine LV cardiomyocytes (isolated from mice age 7–9 weeks). Scale bar=5 µm. **C**, Electron micrograph and schematic of sarcomere (modified from Garfinkel et al[39] with permission). Z-discs (Z), M-band (M), A-band (A), I-band (I). **D**, Electron micrographs demonstrate organized sarcomeres in WT and *Alpk3*$^{+/-}$ murine LV cardiomyocytes, whereas sarcomeres in *Alpk3*$^{-/-}$ murine LV cardiomyocytes have less organized M-bands, loss of the central dark M-band stripe (**C**), and increased electron density between thick filaments in the A-band region (**lower**). LV tissues isolated from mice age 4 to 8 weeks. Scale bar (**top 2 rows**)=500 nm; (**bottom row**), 50 nm. ALPK3 indicates α-kinase 3; eGFP, endogenous GFP; hiPSC-CM, human induced pluripotent stem cell–derived cardiomyocyte; MYOM2, myomesin-2; TTN, titin; and WT, wild type.

human patients (Figure 3E, mean LV posterior wall thickness age 51 to 90 weeks: *Alpk3*$^{+/-}$ (n=20)=0.95 mm versus WT (n=16)=0.77 mm; $P=7.0\times10^{-10}$).

Proteomic analyses of murine LV tissues at postnatal day 8 (n=5789 proteins) identified no differences between *Alpk3*$^{+/-}$ and WT (0 DE proteins), whereas *Alpk3*$^{-/-}$ had 38 DE proteins (Supplemental Data S3). It is remarkable that, similar to *ALPK3*$^{del/ins}$, *ALPK3*$^{del/del}$, and *ALPK3*$^{dIC/dIC}$ hiPSC-CMs, the most significant DE proteins in mice included MYOM1, MYOM2, and MYH7 (Figure 3G), which had increased levels in *Alpk3*$^{-/-}$ relative to WT LV tissues. Western blotting further confirmed that both splice isoforms of MYOM1 were increased in *Alpk3*$^{-/-}$ LV tissues compared with WT (Figure S5C). Western blots identified no significant differences in MuRF1 levels in *Alpk3*$^{-/-}$ mouse LV tissues relative to WT, whereas CAPN3 levels were increased (Figure S6, 1.8-fold increase, $P=4.3\times10^{-2}$).

Phosphoproteomic studies of mouse LV tissues (n=3165 phosphopeptides with corresponding protein levels) showed no significant differences in phosphorylation between *Alpk3*$^{+/-}$ and WT and minimal differences (n=38 differentially phosphorylated peptides, 21 with reduced phosphorylation) between *Alpk3*$^{-/-}$ and WT tissues (Supplemental Data S2). None of these differentially phosphorylated sites in *Alpk3*$^{-/-}$ mouse LV tissues were shared with *ALPK3*$^{ns/del}$ or *ALPK3*$^{del/del}$ hiPSC-CMs, as might be expected if ALPK3 were a catalytically active kinase with specific substrates (Supplemental Data S2). These findings suggested that the changes in phosphorylation in the mouse *Alpk3*$^{-/-}$ LV tissues likely reflect indirect changes in phosphorylation secondary to loss of ALPK3 protein expression rather than loss of ALPK3 catalytic activity.

Analysis of Myomesin Protein Expression in *ALPK3* Human Patient Tissues

Having demonstrated that *ALPK3* loss-of-function dysregulated myomesin proteins in both hiPSC-CMs and mice, we examined myomesin protein expression in LV tissues from 2 human patients with *ALPK3* compound heterozygous variants compared with 5 healthy adult LV tissues (genotypes and clinical characteristics summarized in Table S2). Western blot analyses revealed significant increases in MYOM1 in ALPK3 patient tissues relative to controls (Figure 3H, 1.6-fold increase, $P=3.3\times10^{-4}$). MYOM2 levels appeared slightly increased but did not meet the threshold for statistical significance (Figure 3H, 1.2-fold increase, $P=0.24$). MuRF1 levels were decreased in 1 of the 2 patient tissues (derived from an adult donor with significant hypertrophy), and CAPN3 levels were increased in both tissues (Figure S6). However, because of the large variability in expression of these proteins among controls and limited sample size, these changes were not statistically significant, precluding definitive conclusions.

Analysis of Myomesin and Thick Filament Transcripts in *ALPK3* Mutant Cardiomyocytes and LV Tissues

To assess whether there were also changes in myomesin, myosin heavy chain, and other sarcomere M-band protein transcripts, we analyzed bulk RNA sequencing from WT and hiPSC-CMs and murine LVs (Table S3, Supplemental Data S1) and single nuclear RNA sequencing from *ALPK3* patient and control LVs (Table S4). In each distinct sample type (hiPSC-CMs, murine LV tissues, human LV tissues), *MYOM1* and *MYOM2* transcripts were increased 1.4- to 1.8-fold in *ALPK3* mutant versus the respective WT controls, but were not statistically significant in the 2 human samples (Tables S3 and S4). The expression of myosin heavy chains was heterogenous. In *ALPK3*$^{ns/del}$ hiPSC-CMs, *MYH7* transcripts were unchanged, whereas *MYH6* transcripts were ~4-fold increased, and in mice and human LV tissues, *MYH7* transcripts were 1.2- to 2-fold increased and *MYH6* transcripts were 1.2- to 2-fold decreased (Tables S3 and S4). From these analyses, we concluded that gene transcription may partially contribute to the increase in myomesin and myosin heavy chain protein levels in *ALPK3* mutant cells and tissues.

ALPK3 Variants Cause Myomesin Accumulation and Disrupt Cardiomyocyte Sarcomere Structure

We used immunofluorescence to examine the localization and abundance of myomesins and ALPK3 in hiPSC-CMs and murine cardiomyocytes. As expected from its sarcomere interactions, MYOM1 staining was detected predominantly at the M-band in WT hiPSC-CMs (Figure 4, Figure S7). By contrast, *ALPK3*$^{ns/del}$ hiPSC-CMs had more intense M-band staining of MYOM1 in

addition to cytoplasmic foci of MYOM1 staining outside the sarcomere and surrounding the nuclear envelope, suggesting protein accumulation (Figure 4, Figure S7). Similar findings were observed in primary ventricular cardiomyocytes isolated from WT and *Alpk3*$^{-/-}$ mice (age 7–9 weeks) in which staining in mutant cardiomyocytes identified nonsarcomeric cytoplasmic foci of Myom1 (Figure 4, Figure S7).

In hiPSC-CMs, antibodies to MYOM2 stained the nuclear envelope, a localization that has not been reported previously, hinting at unrecognized developmental roles for MYOM2 in immature cardiomyocytes. Relative to WT, MYOM2 staining of *ALPK3*$^{ns/del}$ hiPSC-CMs was distributed more diffusely throughout the nucleus (Figure 5A). Although Myom2 antibody staining of isolated murine LV cardiomyocytes (age 7–9 weeks) had poor signal-to-noise intensity, some striated staining at M-bands was observed in WT cells, but no striations were discerned in *Alpk3*$^{-/-}$ murine cardiomyocytes (Figure 5B).

The altered localization of myomesins in *Alpk3*$^{ns/del}$ prompted a more detailed examination of in vivo sarcomere structures (Figure 5C). Electron microscopy of LV tissues (perfused with fixative in cardioplegic buffer to promote sarcomere relaxation) showed organized sarcomeres with discrete M-, A-, and I-bands in WT and *Alpk3*$^{+/-}$ mice (Figure 5D). In contrast, M-bands in *Alpk3*$^{-/-}$ mice were less aligned and had enhanced electron density between the thick filaments in the peri M-band and A-band regions (Figure 5D), possibly because of mislocalized and accumulated M-band and thick filament proteins.

ALPK3 Colocalizes With Myomesin Proteins in the Nucleus and the Sarcomere in hiPSC-CMs

ALPK3 has a nuclear localization sequence and localizes primarily to the nucleus in transfected fibroblast-like COS (CV-1 [simian] in origin, and carrying the SV40 genetic material) cells,[40] but its subcellular localization in cardiomyocytes was undetermined. Because several commercial ALPK3 antibodies were nonspecific (on the basis of indistinguishable staining of *ALPK3*$^{ns/del}$ and WT hiPSC-CMs), we produced an epitope tagged ALPK3 construct (ALPK3-FLAG) that was expressed in hiPSC-CMs by transient transfection. Using an anti-FLAG antibody (Figure 6A), we detected ALPK3 at both the M-band (Figure 6B) and the nuclear envelope (Figure 6C) in hiPSC-CMs. Depth-encoded projections of confocal z-slices confirmed that the majority of nuclear ALPK3 signal was at the nuclear envelope, as opposed to within the nucleus (Figure 6D).

Close examination of MYOM1 staining showed that in addition to its localization at the M-band (Figure 6E), some hiPSC-CMs also have MYOM1 at the nuclear envelope (Figure 6E) and within the nucleus (Figure 6F). Although MYOM2 antibodies only stained the nuclear envelope in hiPSC-CMs (Figure 6G), the relative expression of MYOM2 in hiPSC-CMs and embryonic LV tissue is low (Figure S5D and S5E). We hypothesized that MYOM2 might undergo a postnatal shift to the M-band when its expression increases. Consistent with this model, increasing MYOM2 expression in hiPSC-CMs by transient transfection of an MYOM2-HA construct led to its prominent localization at the M-band (Figure 6H). Coimmunostaining confirmed that ALPK3-FLAG precisely colocalized with both MYOM1 and MYOM2-HA (Figure S8).

Ectopically expressed ALPK3-FLAG and MYOM2-HA were found to coimmunoprecipitate in HEK293T cells, indicating the presence of a direct interaction between these proteins. ALPK3-FLAG and MYOM1-HA did not coimmunoprecipitate in HEK293T cells but colocalized within cells (Figure S8), possibly because these proteins interact indirectly, or require additional cardiomyocyte-specific binding partners or factors that are not present in HEK293T cells.

Together, these analyses show that ALPK3, MYOM1, and MYOM2 form a critical protein network in both the nucleus and the sarcomere M-band at various stages in cardiomyocyte development and demonstrate that loss of *ALPK3* causes the profound mislocalization and accumulation of myomesin and thick filament proteins.

DISCUSSION

We report the biochemical and molecular functions of ALPK3 and provide insights into the pathogenesis of *ALPK3* cardiomyopathy. Our investigations revealed that ALPK3 lacks catalytic activity, establishing it as the first pseudokinase of the α-kinase family. Using multiple model systems including hiPSC-CMs, mice, and human patient tissues, we demonstrate that ALPK3 is essential for ensuring the proper localization and expression of proteins including myomesins in both the nucleus and sarcomere, the absence of which compromises cardiomyocyte structure and function.

ALPK3 had not been previously identified as a pseudokinase, although distinguishing these from active kinases using bioinformatic approaches remains a difficult and imperfect science. By comparing the α-kinase domains in ALPK3 with other human α-kinases and their orthologs, we found 4 evolutionarily conserved residues (G1725, K1729, Q1769, N1797) that were all variant in ALPK3. Our phosphoproteomic studies of *ALPK3*$^{dIC/dIC}$ hiPSC-CMs, which altered the conformation of the kinase domain, *ALPK3*$^{sIC/sIC}$, which targeted the predicted aspartate residue critical for catalysis, and massive overexpression of ALPK3 in HEK293T cells indicated that none of these perturbations significantly affected phosphorylation across the proteome. Given the perfect conservation of 4 residues within all other α-kinase family members except ALPK3, we infer that the variation of these residues during evolution may have

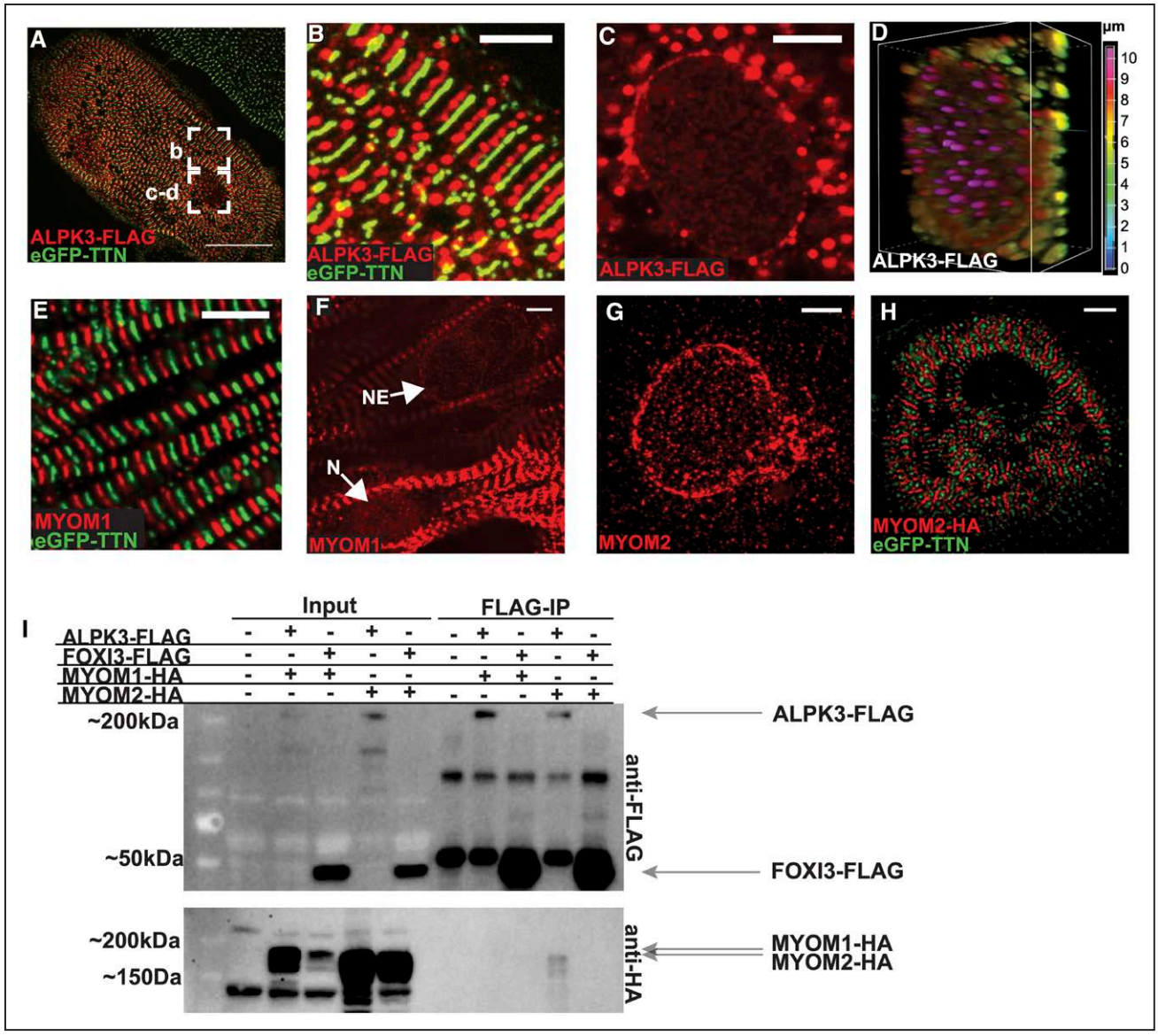

Figure 6. Colocalization and protein interactions of ALPK3 and myomesins.
Confocal micrographs of hiPSC-CMs expressing eGFP-TTN (green) and ALPK3-FLAG (probed with anti-FLAG antibody; red). **A**, ALPK3-FLAG introduced by transient plasmid transfection into hiPSC-CMs expressing eGFP-TTN. Scale bar=25 µm. **B**, Magnified regions of **A** display ALPK3-FLAG (red) localizing to sarcomere M-bands between Z-discs (green, eGFP-TTN). Scale bar=5 µm. **C**, ALPK3-FLAG (red) localizes to nuclear envelope. Scale bar=5 µm. **D**, Depth-encoded (Z-stack) maximum intensity projection of nucleus (**C**) showing ALPK3 localization at nuclear envelope. **E**, MYOM1, stained with anti-myomesin 1 antibody (red) localizes to M-bands between Z-discs (green, eGFP-TTN). Scale bar=5 µm. **F**, MYOM1 (red) is also found at the nucleus (N) and nuclear envelope (NE). Scale bar=5 µm. **G**, MYOM2, stained with anti-myomesin 2 antibody (red), localizes to the nuclear envelope. Scale bar=5 µm. **H**, hiPSC-CMs transfected with plasmid expressing MYOM2-HA (red) shows MYOM2 at M-bands between Z-discs (green, eGFP-TTN). Scale bar=5 µm. **I**, Immunoprecipitation (IP) studies of ALPK3-FLAG, FOXI3-FLAG (negative control), and myomesins (MYOM1-HA, MYOM2-HA) in transfected HEK293T cells. IP of ALPK3-FLAG results in pulldown of MYOM2-HA. ALPK3 indicates α-kinase 3; eGFP, endogenous GFP; hiPSC-CM, human induced pluripotent stem cell–derived cardiomyocyte; MYOM1, myomesin-1; MYOM2, myomesin-2; and TTN, titin.

inactivated ALPK3 catalytic functions and enabled the kinase domain to assume other, noncatalytic functions.

By exploring these functions in both human and mouse cardiomyocytes, we identified a novel subcellular localization of ALPK3 at the sarcomere M-band and the nuclear envelope and revealed that ALPK3 is critical for ensuring the proper localization of myomesin proteins at these regions. The dysregulation and mislocalization of myomesin proteins that occurred with *ALPK3*$^{dIC/dIC}$ and *ALPK3*$^{ins/del}$ variants indicate that the α-kinase domain may function in recruiting myomesin proteins at these structures, as supported by coimmunoprecipitation experiments that showed a direct interaction between ALPK3 and MYOM2. Myomesins are spring-like proteins containing multiple α-helices that undergo rapid unfolding and refolding under axial forces, minimizing M-band

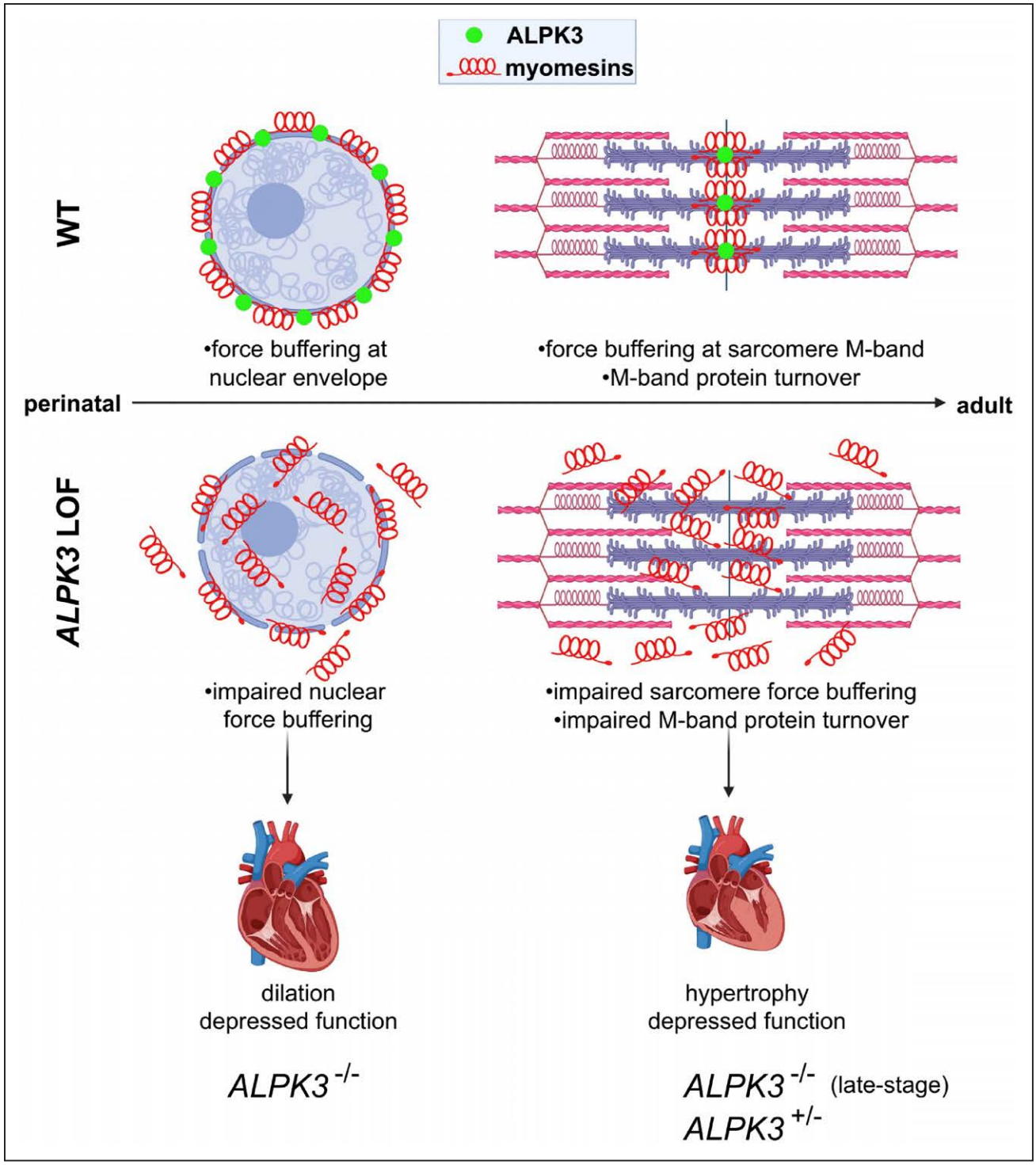

Figure 7. Modelfor ALPK3 function in cardiomyocytes.
Top, In WT cardiomyocytes, ALPK3 (green) is found in both the nuclear envelope and the sarcomere M-band together with myomesin proteins (red). Myomesins are spring-like proteins with multiple distensible α-helical domains that can buffer mechanical forces. In the perinatal period, myomesins are found in the nuclear envelope, and later in development, they are found in the sarcomere. **Bottom**, *ALPK3* loss-of-function (LOF) variants cause myomesin proteins to mislocalize and accumulate, compromising nuclear and sarcomeric force buffering, leading to cardiomyocyte dysfunction, ventricular dilatation, and rapid heart failure. Emergence of hypertrophy in neonatal survivors and adults with *ALPK3* heterozygous variants may be caused by the dysregulation of additional M-band proteins including depressed MuRF1 and increased CAPN3 levels, which participate in sarcomere protein turnover. ALPK3 indicates α-kinase 3; CAPN3, calpain 3; MuRF1, muscle RING-finger protein 1; and WT, wild type.

force imbalances generated by opposing myosins during sarcomere contraction.[33,34,41] Given these functions, we propose that *ALPK3* variants that cause mislocalization of myomesins may compromise force buffering and lead to impaired structural integrity of the sarcomere, as was seen by examination of *Alpk3*$^{-/-}$ murine LV tissues by electron microscopy. Rare loss-of-function and deleterious missense variants in *MYOM1* and *MYOM2* are associated with human cardiomyopathies, and knockout of *MYOM1* in hiPSC-CMs and *MYOM2* in *Drosophila* have deleterious effects on sarcomere structure and contractility, further indicating the functional importance of these proteins in cardiomyocytes.[42–44]

Although the importance of myomesin proteins in the sarcomere is well established, the nuclear roles of these proteins are not well understood.[45] Although MYOM1 was first recognized as a nuclear protein in studies of newborn rat cardiomyocytes, we further demonstrated that MYOM1, MYOM2, and ALPK3 are all present in the nuclear envelope of hiPSC-CMs, suggesting an early developmental function of this protein network. The importance of the nuclear envelope for cardiomyocyte function is demonstrated by loss-of-function variants in lamin A/C (*LMNA*), which compromise nuclear envelope integrity and lead to dilated cardiomyopathy.[46,47] We speculate that the insertion of myomesins in the nuclear envelope in developing cardiomyocytes may also confer force buffering functions, thereby protecting the nucleus in the neonatal period when cardiomyocytes must divide and replicate while maintaining cardiac contraction. Thus, myomesin mislocalization in both the nucleus and sarcomere may ultimately impair cardiomyocyte structure and function, culminating in depressed contractility and ventricular dilatation (Figure 7). Future studies to specifically ablate the nuclear or sarcomeric populations of ALPK3 and myomesins at various developmental time points may help to discern the precise roles of these proteins at either structure.

We suspect that the hypertrophy caused by *ALPK3* cardiomyopathy in surviving newborns with recessive pathogenic variants and adults with heterozygous pathogenic variants may be related to additional roles of ALPK3 in directly or indirectly regulating sarcomere protein turnover at the M-band. Another M-band pseudokinase domain is encoded by the C terminus of TTN, which recruits several proteins important in sarcomere protein turnover, including the autophagy cargo receptor (encoded by *NBR1*), p62 (encoded by *SQSTM*), and MuRF1 (encoded by *TRIM63*) complex, which degrades thick filament proteins,[37] and the cysteine protease calpain-3 (encoded by CAPN3), which cleaves and releases myofibrillar proteins for ubiquitin-proteasome-dependent degradation.[48–50] We found that MuRF1 and CAPN3 were both DE in *ALPK3*$^{dIC/dIC}$ and *ALPK3*$^{ns/del}$ hiPSC-CMs, suggesting that loss of the ALPK3 kinase domain may also dysregulate this protein turnover machinery. The dysregulation of MuRF1 is particularly remarkable, because this E3-ubiquitin ligase targets contractile proteins. Like ALPK3, MURF1 expression is developmentally regulated, increasing late in gestation to achieve a maximal level that is maintained throughout life,[51] and can be found in both the nucleus and the M-band.[52] Augmentation of MuRF1 expression promotes muscle atrophy,[37] whereas reduction in MuRF1 expression caused by rare recessive human pathogenic variants in *TRIM63* promotes hypertrophic remodeling.[53] We speculate that the reduced levels of MuRF1 protein (despite normal transcripts) in *ALPK3*$^{ns/del}$ and *ALPK3*$^{dIC/dIC}$ hiPSC-CMs could reflect its heightened consumption, which may contribute to the accumulation of M-band and thick filament proteins that was observed in *ALPK3* mutant hiPSC-CMs. This could explain the eventual emergence of hypertrophy in surviving neonates who initially present with cardiac dilation, and in adults with heterozygous *ALPK3* variants[6] (Figure 7).

In summary, our studies identify ALPK3 as an α-pseudokinase that regulates the expression and localization of critical proteins including myomesins in both the sarcomere M-band and the nuclear envelope of cardiomyocytes. Further studies to characterize the ALPK3-MYOM1-MYOM2 protein network across developmental stages will provide further insights into the roles of these proteins in the establishment and maintenance of cardiomyocyte structure and function.

ARTICLE INFORMATION

Received February 16, 2022; accepted September 19, 2022.

Affiliations

Department of Genetics (R.A., H.W., Q.Z., D.R., C.T., A.S., A.C.T., M.L., J.G., S.R.D., J.G.S., C.E.S.), Department of Cell Biology (J.A.P., S.P.G.), Harvard Medical School, Boston, MA. Radcliffe Department of Medicine (C.T.), Wellcome Centre for Human Genetics (C.T.), University of Oxford, United Kingdom. Board of Governors Regenerative Medicine Institute (A.S.), Smidt Heart Institute (A.S.), Department of Biomedical Sciences (A.S.), Cedars-Sinai Medical Center, Los Angeles, CA. Division of Cardiovascular Medicine, Brigham and Women's Hospital, Boston, MA (C.E.S.). Howard Hughes Medical Institute, Chevy Chase, MD (C.E.S.).

Acknowledgments

The authors thank the Microscopy Resources on the North Quad (MicRoN) core at Harvard Medical School for assistance with imaging studies. Electron microscopy imaging, consultation, and services were performed in the Harvard Medical School Electron Microscopy Facility.

Sources of Funding

This work was supported in part by the National Heart, Lung, and Blood Institute (F30HL147389 to R.A.), National Institutes of Health/National Institute of General Medical Sciences (R01 GM132129 to J.A.P. and GM97645 to S.P.G.), Sir Henry Wellcome Postdoctoral Fellowship from the Wellcome Trust (206466/Z/17/Z to C.N.T.), British Heart Foundation Centre of Research Excellence, Oxford (RE/18/3/34214 to C.N.T.), National Heart, Blood, and Lung Institute and Leducq Foundation (HL084553 and HL080494 to J.G.S. and C.E.S.), and Howard Hughes Medical Institute (to C.E.S.).

Disclosures

C.N.T. works as consultant for Myokardia Inc. J.G.S. and C.E.S. are founders of Myokardia (a Bristol Myers Squibb Subsidiary) and consultants for Maze and BridgeBio. C.E.S. serves on the Merck Board of Directors. None of these

companies provided any support or input into this article. The other authors report no conflicts.

Supplemental Material

Tables S1–S4
Figures S1–S8
Data Sets (Excel) S1–S4
Data Sets (PDF) S5 and S6

REFERENCES

1. Lee TM, Hsu DT, Kantor P, Towbin JA, Ware SM, Colan SD, Chung WK, Jefferies JL, Rossano JW, Castleberry CD, et al. Pediatric cardiomyopathies. *Circ Res.* 2017;121:855–873. doi: 10.1161/CIRCRESAHA.116.309386
2. Seidman JG, Seidman C. The genetic basis for cardiomyopathy. *Cell.* 2001;104:557–567. doi: 10.1016/s0092-8674(01)00242-2
3. Almomani R, Verhagen JMA, Herkert JC, Brosens E, van Spaendonck-Zwarts KY, Asimaki A, van der Zwaag PA, Frohn-Mulder IME, Bertoli-Avella AM, Boven LG, et al. Biallelic truncating mutations in ALPK3 cause severe pediatric cardiomyopathy. *J Am Coll Cardiol.* 2016;67:515–525. doi: 10.1016/j.jacc.2015.10.093
4. Al Senaidi K, Niranjan S, Maryam J, Al A, Khalid F, Al-maawali A. Phenotypic spectrum of ALPK3-related cardiomyopathy. *Am J Mol Genet.* 2019;179:1235–1240. doi: 10.1002/ajmg.a.61176
5. Cağlayan AO, Sezer RG, Kaymakcalan H, Ulgen E, Yavuz T, Baranoski JF, Bozaykut A, Serin Harmanci A, Yalcin Y, Youngblood MW, et al. Alpk3 gene mutation in a patient with congenital cardiomyopathy and dysmorphic features. *Cold Spring Harbor Mol Case Stud.* 2017;3:1–9.
6. Herkert JC, Verhagen JMA, Yotti R, Phelan DG, James PA, Brown NJ, Stutterd C, Macciocca I, Leong KE, Marian LC, et al. Expanding the clinical and genetic spectrum of ALPK3 variants: phenotypes identified in pediatric cardiomyopathy patients and adults with heterozygous variants. *Am Heart J.* 2020;225:108–119. doi: 10.1016/j.ahj.2020.03.023
7. Jaouadi H, Kraoua L, Chaker L, Atkinson A, Delague V, Levy N, Benkhalifa R, Mrad R, Abdelhak S, Zaffran S. Novel ALPK3 mutation in a Tunisian patient with pediatric cardiomyopathy and facio-thoraco-skeletal features. *J Hum Genet.* 2018;63:1077–1082. doi: 10.1038/s10038-018-0492-1
8. Phelan DG, Anderson DJ, Howden SE, Wong RCB, Hickey PF, Pope K, Wilson GR, Pébay A, Davis AM, Petrou S, et al. ALPK3-deficient cardiomyocytes generated from patient-derived induced pluripotent stem cells and mutant human embryonic stem cells display abnormal calcium handling and establish that ALPK3 deficiency underlies familial cardiomyopathy. *Eur Heart J.* 2016;37:2586–2590. doi: 10.1093/eurheartj/ehw160
9. Lopes LR, Garcia-Hernández S, Lorenzini M, Futema M, Chumakova O, Zateyshchikov D, Isidoro-Garcia M, Villacorta E, Escobar-Lopez L, Garcia-Pavia P, et al. Alpha-protein kinase 3 (ALPK3) truncating variants are a cause of autosomal dominant hypertrophic cardiomyopathy. *Eur Heart J.* 2021;42:3063–3073. doi: 10.1093/eurheartj/ehab424
10. Drennan D, Ryazanov AG. Alpha-kinases: analysis of the family and comparison with conventional protein kinases. *Prog Biophys Mol Biol.* 2004;85:1–32. doi: 10.1016/S0079-6107(03)00060-9
11. Yamaguchi H, Matsushita M, Nairn AC, Kuriyan J. Crystal structure of the atypical protein kinase domain of a TRP channel with phosphotransferase activity. *Mol Cell.* 2001;7:1047–1057. doi: 10.1016/s1097-2765(01)00256-8
12. Middelbeek J, Clark K, Venselaar H, Huynen MA, Van Leeuwen FN. The alpha-kinase family: an exceptional branch on the protein kinase tree. *Cell Mol Life Sci.* 2010;67:875–890. doi: 10.1007/s00018-009-0215-z
13. Hosoda T, Monzen K, Hiroi Y, Oka T, Takimoto E, Yazaki Y, Nagai R, Komuro I. A novel myocyte-specific gene Midori promotes the differentiation of P19CL6 cells into cardiomyocytes. *J Biol Chem.* 2001;276:35978–35989. doi: 10.1074/jbc.m100485200
14. Van Sligtenhorst I, Ding Z-M, Shi Z-Z, Read RW, Hansen G, Vogel P. Cardiomyopathy in α-kinase 3 (ALPK3)–deficient mice. *Vet Pathol.* 2012;49:131–141. doi: 10.1177/0300985811402841
15. Sharma A, Toepfer CN, Schmid M, Garfinkel AC, Seidman CE. Differentiation and contractile analysis of GFP-sarcomere reporter hiPSC-cardiomyocytes. *Curr Protoc Hum Genet.* 2018;96:21.12.1–21.12.12. doi: 10.1002/cphg.53
16. Litviňuková M, Talavera-López C, Maatz H, Reichart D, Worth CL, Lindberg EL, Kanda M, Polanski K, Heinig M, Lee M, et al. Cells of the adult human heart. *Nature.* 2020;588:466–472. doi: 10.1038/s41586-020-2797-4
17. Sievers F, Wilm A, Dineen D, Gibson TJ, Karplus K, Li W, Lopez R, Thompson JD, Higgins DG, Mcwilliam H, et al. Fast, scalable generation of high-quality protein multiple sequence alignments using Clustal Omega. *Mol Syst Biol.* 2011;7:1–6. doi: 10.1038/msb.2011.75
18. Waterhouse AM, Procter JB, Martin DMA, Clamp M, Barton GJ. Jalview Version 2 — a multiple sequence alignment editor and analysis workbench. *Bioinformatics.* 2009;25:1189–1191. doi: 10.1093/bioinformatics/btp033
19. Sali A, Blundell T. Comparative protein modeling by satisfaction of spatial restraints. *J Mol Biol.* 1993;234:779–815. doi: 10.1006/jmbi.1993.1626
20. Pettersen EF, Goddard TD, Huang CC, Couch GS, Greenblatt DM, Meng EC, Ferrin TE. UCSF chimera — a visualization system for exploratory research and analysis. *J Comput Chem.* 2004;25:1605–1612. doi: 10.1002/jcc.20084
21. Sharma A, Toepfer CN, Ward T, Wasson L, Agarwal R, Conner DA, Hu JH, Seidman CE. CRISPR/Cas9-mediated fluorescent tagging of endogenous proteins in human pluripotent stem cells. *Curr Protoc Hum Genet.* 2018;96:21.11.1–21.11.20. doi: 10.1002/cphg.52
22. Yang L, Yang JL, Byrne S, Pan J, Church GM. CRISPR/Cas9-directed genome editing of cultured cells. *Curr Protoc Mol Biol.* 2014;2014:31.1.1–31.1.17. doi: 10.1002/0471142727.mb3101s107
23. Lian X, Zhang J, Azarin SM, Zhu K, Hazeltine LB, Bao X, Hsiao C, Kamp TJ, Palecek SP. Directed cardiomyocyte differentiation from human pluripotent stem cells by modulating Wnt/β-catenin signaling under fully defined conditions. *Nat Protoc.* 2013;8:162–175. doi: 10.1038/nprot.2012.150
24. Toepfer CN, Sharma A, Cicconet M, Garfinkel AC, Mücke M, Neyazi M, Willcox JAL, Agarwal R, Schmid M, Rao J, et al. SarcTrack an adaptable software tool for efficient large-scale analysis of sarcomere function in hiPSC-cardiomyocytes. *Circ Res.* 2019;124:1172–1183. doi: 10.1161/CIRCRESAHA.118.314505
25. Navarrete-Perea J, Yu Q, Gygi SP, Paulo JA. Streamlined tandem mass tag (SL-TMT) protocol: an efficient strategy for quantitative (phospho) proteome profiling using tandem mass tag-synchronous precursor selection-MS3. *J Proteome Res.* 2018;17:2226–2236. doi: 10.1021/acs.jproteome.8b00217
26. Agarwal R, Paulo JA, Toepfer CN, Ewoldt JK, Sundaram S, Chopra A, Zhang Q, Gorham J, DePalma SR, Chen CS, et al. Filamin C cardiomyopathy variants cause protein and lysosome accumulation. *Circ Res.* 2021;129:751–766. doi: 10.1161/CIRCRESAHA.120.317076
27. Nadelmann ER, Gorham JM, Reichart D, Delaughter DM, Wakimoto H, Lindberg EL, Litviňukova M, Maatz H, Curran JJ, Ischiu Gutierrez D, et al. Isolation of nuclei from mammalian cells and tissues for single-nucleus molecular profiling. *Curr Protoc.* 2021;1:1–18. doi: 10.1002/cpz1.132
28. Sharma A, Toepfer CN, Schmid M, Garfinkel AC, Seidman CE. Differentiation and contractile analysis of GFP-sarcomere reporter hiPSC-cardiomyocytes. *Curr Protoc Hum Genet.* 2018;21.12.1–21.12.12. doi: 10.1002/cphg.53
29. Toepfer CN, Wakimoto H, Garfinkel AC, Mcdonough B, Liao D, Jiang J, Tai AC, Gorham JM, Lunde IG, Lun M, et al. Hypertrophic cardiomyopathy mutations in MYBPC3 dysregulate myosin. *Sci Transl Med.* 2019;11:eaat1199. doi: 10.1126/scitranslmed.aat1199
30. Wang X, Osinska H, Dorn GW, Nieman M, Lorenz JN, Gerdes AM, Witt S, Kimball T, Gulick J, Robbins J. Mouse model of desmin-related cardiomyopathy. *Circulation.* 2001;103:2402–2407. doi: 10.1161/01.cir.103.19.2402
31. Love M, Huber W, Anders S. Moderated estimation of fold change and dispersion for RNA-seq data with DESeq2. *Genome Biol.* 2014;15:1–21. doi: 10.1186/s13059-014-0550-8
32. Agarkova I, Perriard J. The M-band: an elastic web that crosslinks thick filaments in the center of the sarcomere. *Trends Cell Biol.* 2005;15:477–485. doi: 10.1016/j.tcb.2005.07.001
33. Auerbach D, Bantle S, Keller S, Hinderling V, Ehler E, Perriard J. Different domains of the M-band protein myomesin are involved in myosin binding and M-band targeting. *Mol Biol Cell.* 1999;10:1297–1308. doi: 10.1091/mbc.10.5.1297
34. Xiao S, Grater F. Molecular basis of the mechanical hierarchy in myomesin dimers for sarcomere integrity. *Biophys J.* 2014;107:965–973. doi: 10.1016/j.bpj.2014.06.043
35. Bogomolovas J, Fleming JR, Franke B, Manso B, Simon B, Gasch A, Markovic M, Brunner T, Knöll R, Chen J, et al. Titin kinase ubiquitination aligns autophagy receptors with mechanical signals in the sarcomere. *EMBO Rep.* 2021;22:e48018. doi: 10.15252/embr.201948018
36. Bogomolovas J, Gasch A, Simkovic F, Rigden DJ, Labeit S, Mayans O. Titin kinase is an inactive pseudokinase scaffold that supports MuRF1 recruitment to the sarcomeric M-line. *Open Biology.* 2014;4:1400411–1400412. doi: 10.1098/rsob.140041
37. Clarke BA, Drujan D, Willis MS, Murphy LO, Corpina RA, Burova E, Rakhilin SV, Stitt TN, Patterson C, Latres E, et al. The E3 ligase MuRF1 degrades

myosin heavy chain protein in dexamethasone-treated skeletal muscle. *Cell Metab*. 2007;2:376–385. doi: 10.1016/j.cmet.2007.09.009
38. Sarparanta J, Charton K, Vihola A, Marchand S, Milic A, Hackman P, Ehler E, Richard I, Udd B. Interactions with M-band titin and calpain 3 Link myospryn (CMYA5) to tibial and limb-girdle muscular dystrophies. *J Biol Chem*. 2010;285:30304–30315. doi: 10.1074/jbc.M110.108720
39. Garfinkel AC, Seidman JG, Seidman CE. Genetic pathogenesis of hypertrophic and dilated cardiomyopathy. *Heart Fail Clin*. 2018;14:13.
40. Hosoda T, Monzen K, Hiroi Y, Oka T, Takimoto E, Yazaki Y, Nagai R, Komuro I. A novel myocyte-specific gene Midori promotes the differentiation of P19CL6 cells into cardiomyocytes. *J Biol Chem*. 2001;276:35978–35989. doi: 10.1074/jbc.m100485200
41. Lange S, Pinotsis N, Agarkova I, Ehler E. The M-band: The underestimated part of the sarcomere. *Biochim Biophys Acta Mol Cell Res*. 2020;1867:118440. doi: 10.1016/j.bbamcr.2019.02.003
42. Auxerre-Plantié E, Nielsen T, Grunert M, Olejniczak O, Perrot A, Özcelik C, Harries D, Matinmehr F, Dos Remedios C, Mühlfeld C, et al. Identification of MYOM2 as a candidate gene in hypertrophic cardiomyopathy and tetralogy of fallot and its functional evaluation in the Drosophila heart. *Dis Model Mech*. 2020;1:15. doi: 10.1242/dmm.045377
43. Hang C, Song Y, Li Y, Zhang S, Chang Y, Bai R, Saleem A, Jiang M, Lu W, Lan F, et al. Knockout of MYOM1 in human cardiomyocytes leads to myocardial atrophy via impairing calcium homeostasis. *J Cell Mol Med*. 2021;25:1661–1676. doi: 10.1111/jcmm.16268
44. Siegert R, Perrot A, Keller S, Behlke J, Michalewska-włudarczyk A, Wycisk A, Tendera M, Morano I, Özcelik C. A myomesin mutation associated with hypertrophic cardiomyopathy deteriorates dimerisation properties. *Biochem Biophys Res Commun*. 2011;405:473–479. doi: 10.1016/j.bbrc.2011.01.056
45. Reddy KB, Fox JEB, Price MG, Kulkarni S, Gupta S, Das B, Smith DM. Nuclear localization of myomesin-1: possible functions. *J Muscle Res Cell Motil*. 2008;29:1–8. doi: 10.1007/s10974-008-9137-x
46. Brayson D, Shanahan CM. Current insights into LMNA cardiomyopathies: existing models and missing LINCs. *Nucleus*. 2017;8:17–33. doi: 10.1080/19491034.2016.1260798
47. Tesson F, Saj M, Uvaize MM, Nicolas H, Płoski R, Bilińska Z. Lamin A/C mutations in dilated cardiomyopathy. *Cardiol J*. 2014;21:331–342. doi: 10.5603/CJ.a2014.0037
48. Kinbara K, Sorimachi H, Ishiura S, Suzuki K. Muscle-specific calpain, p94, interacts with the extreme C-terminal region of connectin, a unique region flanked by two immunoglobulin C2 motifs. *Arch Biochem Biophys*. 1997;342:99–107. doi: 10.1006/abbi.1997.0108
49. Kramerova I, Kudryashova E, Venkatraman G, Spencer MJ. Calpain 3 participates in sarcomere remodeling by acting upstream of the ubiquitin – proteasome pathway. *Hum Mol Genet*. 2005;14:2125–2134. doi: 10.1093/hmg/ddi217
50. Sorimachi H, Kinbara K, Kimura S, Takahashi M, Sasagawa N, Sorimachi N, Shimada H, Tagawa K, Suzuki K. Muscle-specific calpain, p94, responsible for limb girdle muscular dystrophy type 2A, associates with connectin through IS2, a p94- specific sequence. *J Biol Chem*. 1995;270:31158–31162. doi: 10.1074/jbc.270.52.31158
51. Perera S, Holt MR, Mankoo BS, Gautel M. Developmental regulation of MURF ubiquitin ligases and autophagy proteins nbr1, p62/SQSTM1 and LC3 during cardiac myofibril assembly and turnover. *Dev Biol*. 2011;351:46–61. doi: 10.1016/j.ydbio.2010.12.024
52. Peris-Moreno D, Taillandier D, Polge C. MuRF1/TRIM63, master regulator of muscle mass. *IJMS*. 2020;21:6663. doi: 10.3390/ijms21186663
53. Salazar-Mendiguchía J, Ochoa JP, Palomino-Doza J, Domínguez F, Díez-López C, Akhtar M, Ramiro-León S, Clemente MM, Pérez-Cejas A, Robledo M, et al; GENESCOPIC Research Group. Mutations in TRIM63 cause an autosomal-recessive form of hypertrophic cardiomyopathy. *Heart*. 2020;106:1342–1348. doi: 10.1136/heartjnl-2020-316913